Statistical mechanics of phase transitions in elastic media with vanishing thermal expansion

Sudip Mukherjee[1,*] and Abhik Basu[2,†]
[1]*Barasat Government College, 10, KNC Road, Gupta Colony, Barasat, Kolkata 700124, West Bengal, India*
[2]*Theory Division, Saha Institute of Nuclear Physics, 1/AF, Bidhannagar, Calcutta 700064, West Bengal, India*

(Received 2 September 2021; accepted 25 March 2022; published 14 November 2022)

We consider a minimal spin model for Ising transitions in an isotropic elastic medium in the zero thermal expansion (ZTE) limit. We set up the elastic theory for this system. We use this theory to identify and study the nature of the fluctuations in the system near the second order phase transitions at T_c in the ZTE limit given by $dT_c/dV = 0$, where V is the system volume, and explore anomalous elasticity. Allowing for the local strain to couple *asymmetrically* or *selectively* with the states of the order parameter, we uncover the dramatic effects of these couplings on the fluctuations of the local displacements near T_c, and also on the nature of the phase transition itself. Near second-order phase transitions and with weak asymmetry in the order parameter–strain couplings, the variance of the displacement fluctuations in two dimensions scale with the system size L in a universal fashion as $[\ln(L/a_0)]^{2/3}$; a_0 is a small-scale cutoff. Likewise, the correlation functions of the difference of the local displacements at two different points separated by r scale as $[\ln(r/a_0)]^{2/3}$ for large r. For stronger selectivity above a finite threshold, this variance diverge as L exceeds beyond a (nonuniversal) size, determined by the model parameters, signaling a transition to a phase with only short-range order or the loss of the positional order of the elastic medium. At dimensions higher than two, for sufficiently weak selectivity, the variance of the displacement fluctuations is L-independent corresponding to long-range order. However, if the selectivity parameters rise beyond a dimension-dependent threshold value, then again the positional order is lost with a concomitant transition to a phase with short-range order. Large values of the order parameter–strain couplings can turn the phase transition into a first order as well. Our theory establishes a *one-to-one correspondence* between the order of phase transitions and anomalous elasticity near the transitions. Our theory should be a useful guide to possible synthesis of appropriate ZTE materials.

DOI: 10.1103/PhysRevE.106.054128

I. INTRODUCTION

Phase transitions are ubiquitous in nature and continue to remain central to the subject of equilibrium statistical mechanics for many decades [1,2]. The Ising model is the simplest model that shows phase transitions between a high temperature (T) disordered phase to a low-T ordered phase at dimensions $d > 1$ [3]. It and its variants have been used to study phase transitions in a wide class of systems, ranging from magnetic phase transitions between the high T paramagnetic to the low T ferromagnetic phase [4] to phase separation transitions from a high-T well-mixed phase to a low-T phase separated state [4,5]. These transitions can be second order through a critical point, or first order with a finite jump in the order parameter [6]. Phase separation transitions and corresponding nucleation and the growth of domains are not only significant from statistical mechanics point of views, these are believed to be of paramount importance in host of naturally occurring phenomena, which are of of nonequilibrium origin, e.g., chemical and biological phenomena. For instance, phase separations of proteins are expected to be of vital importance in living biological cells [7].

Elastic media (e.g., crystals) are broken symmetry phases of systems with continuous translational invariance. These are characterized by the broken symmetry Goldstone modes or acoustic phonons [6,8], which are *massless* or long-lived fluctuations. At three dimensions (3D), variance $\langle[\mathbf{u}(\mathbf{x})]^2\rangle$ of the local displacements $u_i(\mathbf{x})$ of the position $\mathbf{x}$ in the undistorted system is a finite constant proportional to T, which means positional long-range order (LRO), whereas in two-dimensional (2D) systems, $\langle[\mathbf{u}(\mathbf{x})]^2\rangle$ grows with the linear system size L as $T \ln(L/a_0)$, setting Boltzmann constant $k_B = 1$, where a_0 is a small-scale cutoff, corresponding to the positional quasi-long-range order (QLRO); the lack of long-range order is a consequence of the Mermin-Wagner-Hohenberg theorem (MWHT) [9]. At higher temperatures, crystals undergo a melting transition into a liquid phase. At 3D, the melting transition is known to be a first-order transition [10]; at 2D, the transition could be either first or second order [11].

Statistical mechanics of phase transitions are well-developed and have a long history of study [1]. How elastic degrees of freedom may conspire with the order parameter to affect the macroscopic behavior of a system near a critical point remains a topic of debate. This brings up the question on the nature of phase transitions in elastic media, and in turn the corresponding scaling of the position fluctuations near the phase transition temperature. However, studies on their mutual interplay are relatively few. For instance, studies

*sudip.bat@gmail.com
†abhik.123@gmail.com, abhik.basu@saha.ac.in

in Ref. [12] showed that the universal critical scaling of the Larkin-Pikin-Sak model is unaffected by a coupling with an elastic continuum. In a seminal study, Ref. [13] showed that generically an isotropic elastic solid gets unstable in the vicinity of an Ising transition at temperature $T = T_c$, except in the case $dT_c/dV = 0$, whence the spin and the elastic degrees of freedom decouple in the long wavelength limit, naturally leading to no mutual effects on each other in their model. Most theoretical studies of phase transitions in elastic media till date either usually concern about the nature and growth of order below the phase transition temperature, or the how the second-order transition of the scalar order parameter (of the undistorted system) belonging to the Ising universality class is affected by the displacement fluctuations coming from the background lattice or network.

Recent studies indicate that order parameter–strain couplings could be important in various phenomenologies. For instance, in a cross-linked, elastic polymer network swollen by a solvent mixture, droplets are found to grow to a fixed size, controlled by the network stiffness [14]. More recent experimental studies have revealed that compressive stresses in a polymer network can suppress phase separation of the solvent that swells it, ultimately stabilizing the mixtures even well beyond the standard liquid-liquid phase-separation boundary [15–18]. Similarly, the order parameter–elasticity interplay is believed to be of importance to understand the ground state and collective excitation of magnetic materials. There has been a growing body of research that considers the various aspects and effects of order parameter–strain coupling in the general context of magnetic materials [19]. In general, in any real magnetic crystal, the interplay between the magnetic and the elastic degrees of freedom should exist. Similarly, in a composite elastic medium (e.g., a binary alloy) or a of composite system made of a two-component fluid and an embedding elastic network (e.g., a polymer network in a mixed fluid), the order parameter–elasticity interplay should be present. In fact, the question of phase separation in an elastic network is believed to be important in cell biological contexts, e.g., liquid-liquid phase separation is proposed as a candidate mechanism for the formation of membraneless compartments in live biological cells [20].

Studies on the statistical mechanics of phase transitions in metamaterials are few and far between. Metamaterials are artificially prepared materials that are designed to have specific properties not found in naturally occurring systems. In this paper, we formulate a generic and experimentally testable theory of phase transitions in a zero thermal expansion (ZTE) medium, coupled with Ising spins. ZTE materials, a particular type of metamaterials that neither expand nor contract over a range of temperature, can be of diverse origin [21], featuring nearly zero thermal expansion behavior. These materials have enormous potential technical applications in wide-ranging fields, e.g., precision engineered parts, microdevices, and functional materials, e.g., thermomechanical actuators. Our theory should be helpful as a guideline in studies on such ZTE systems. We focus on a ferromagnetic Ising model with nearest neighbor interactions, defined on a deformable lattice. We show that the fluctuations near phase transitions in such media can behave very differently from conventional systems with finite thermal expansion. While the scalar order parameter field for the Ising model in the limit of a rigid lattice undergoes a second-order universality class belonging to the Ising universality class, we generalize the scope of our study by allowing the order parameter–strain tensor couplings to break the Ising symmetry of the order parameter. In other words, the local strain couples with the order parameter *selectively* and *asymmetrically*, depending upon the "two states" (i.e., two different signs) of the Ising order parameter. This can be generically present, e.g., in a binary fluid mixture, or in biologically relevant systems where the embedding elastic network can chemically interact with the two fluid components in different ways, or in a binary alloy, where the local deformability can explicitly depend upon the excess or deficit of one or the other component.

Specifically, in this work we schematically consider a ferromagnetic Ising model grafted on Hookean-like spring model for an isotropic elastic medium, e.g., a gel. The spin-lattice interactions are chosen in such a way to ensure vanishing thermal expansions, and correspond to a second-order phase transition belonging to the Ising universality class with a critical temperature T_c. We construct the Landau-Ginzburg theory of phase transitions in this model. We explore anomalous elasticity near phase transitions in this model, that arises due to the interplay between the local strain and Ising-like order parameter fluctuations in elastic media. In this work, we focus on systems with *zero thermal expansions*, which in our model implies $dT_c/dV = 0$ [13]. To generalize the scope of our study, we allow for the local strain to couple selectively or asymmetrically with the states of the order parameter, which breaks the Ising symmetry of the system through these selectivity-dependent order parameter–strain couplings. This is a situation that can potentially arise in soft matter systems, e.g., in elastic networks immersed in a binary fluid. Our most surprising result is that unexpected anomalous behavior of the elastic modulii ensues near T_c, in contrast to the predictions in Ref. [13]. We show that in 2D, the elastic modulii *either stiffen* significantly, diverging *logarithmically* in the wave vector q in the thermodynamic limit $q \to 0$ for *weak selectivity*, or *softens* for *strong selectivity*, vanishing at finite length scales indicating selectivity-induced structural phase transitions to a phase with short-range order (SRO). At 3D, with sufficiently weak selectivity, the elasticity near T_c is statistically identical to that away from T_c. However, with stronger selectivity above a finite threshold, the elastic modulii soften and disappear at finite length scales suggesting structural phase transitions like its 2D counterparts, near T_c. Last, the order parameter–strain couplings can even turn the second-order transition of the rigid lattice system a *first-order transition* in all dimensions. In this case, the elastic modulii shows *finite jumps* across the first-order transition temperature. In what follows below, we interchangeably use "ZTE" and "$dT_c/dV = 0$." A brief account of these results is available in the associated short paper [22].

The remainder of this article is organized as follows. In Sec. II, we summarize our principal results. In Sec. III we present our microscopic model, and formulate its elastic theory near the phase transition by setting up the corresponding coarse-grained Landau-Ginzburg (LG) free energy. Then in Sec. IV, we discuss the properties at the harmonic order of the free energy. Next, in Sec. V, we analyze the anharmonic

effects in 2D and $d > 2$ systems. Then in Sec. VI, we discuss how the transition can be turned into a first-order one. In Sec. VII, we set up the correspondence between the order of the transitions and the local displacement fluctuations. We summarize our results and discuss possible future directions in Sec. VIII. The parameters in this paper, and the equations defining them (where ever applicable), are summarized in the glossary that constitutes Appendix A. Many technical details are available for the interested reader in the subsequent Appendices.

II. SUMMARY OF THE TECHNICAL RESULTS

We consider Ising spins on a Hookean spring-like model for an isotropic gel. The spin-spring interactions are such that the model has ZTE. We study this system by constructing an LG free-energy functional, subject to ZTE, in which we describe an elastic medium with a local displacement field $\mathbf{u}(\mathbf{x})$ of a point $\mathbf{x}$ in the undistorted system, coupled with an Ising-like continuum order parameter field $\phi(\mathbf{x})$. We formally define a displacement field $\mathbf{u}(\mathbf{x})$ that describes the local distortion of the elastic medium, such that $\mathbf{R}(\mathbf{x}) \equiv [\mathbf{x} + \mathbf{u}(\mathbf{x})]$ denotes the new, post-fluctuation coordinates in the medium that was originally located at $\mathbf{x}$. Here, $\mathbf{x} = (x, y)$ for a 2D system, and $\mathbf{x} = (x, y, z)$ for a corresponding 3D realization [6].

After dropping terms that are irrelevant in the renormalization group (RG) sense, the free-energy functional $\mathcal{F}$ invariant under a constant shift of $\mathbf{u}$, as appropriate for this system is

$$\mathcal{F} = \int d^d x \Big[\frac{r}{2}\phi^2 + \frac{1}{2}(\nabla\phi)^2 + v\phi^4 + \mu\big(\nabla_i u_j^T\big)^2 + \frac{\tilde{\lambda}}{2}\big(\nabla_i u_j^L\big)^2 + (g_1\phi^2 + \bar{g}_1\phi)\big(\nabla_i u_j^T\big)^2 + (g_2\phi^2 + \bar{g}_2\phi)\big(\nabla_i u_j^L\big)^2 \Big], \quad (1)$$

where, $r = 0$ is the mean-field critical point in the rigid lattice limit, $u_i^L(\mathbf{x})$ and $u_i^T(\mathbf{x})$ are the inverse Fourier transforms of $u_i^L(\mathbf{q})$ and $u_i^T(\mathbf{q})$. Here, $\mathbf{u}^L(\mathbf{q})$ and $\mathbf{u}^T(\mathbf{q})$ are the projections of $\mathbf{u}(\mathbf{q})$ along and normal to the wave vector $\mathbf{q}$. Couplings $\bar{g}_1$ and $\bar{g}_2$ manifestly break the Ising symmetry of the problem, and are the *selectivity parameters*, since their contributions to $\mathcal{F}$ depend upon the sign of ϕ. Last, μ and $\tilde{\lambda}$ are, respectively, the shear and bulk modulii of the system.

We study the fluctuations in the system corresponding to $\mathcal{F}$ in Eq. (1). Our principal results are given below.

In systems with selectivity, i.e., with nonzero $\bar{g}_1$, $\bar{g}_2$, the transition is generically first order similar to the liquid-gas first order transition. However, again like a liquid-gas transition a second order transition with a critical point at T_c can be accessed.

A. Results on 2D systems

We show that at 2D with weak selectivity (i.e., weak $\bar{g}_1$ and $\bar{g}_2$) such a thin elastic sheet can significantly stiffen close to the critical point T_c of the ordering transition, a property not found in a pure (one component) system, or away from critical points. In particular, both μ and $\tilde{\lambda}$, the shear and bulk modulii respectively, acquire scale-dependence, diverging as $[\ln(\Lambda/q)]^{1/3}$ in the long wavelength limit, which implies *anomalous elasticity*; here Λ is an upper wave-vector cutoff. This is analogous to anomalous elasticity in 3D equilibrium smectics [23]. As a result, the variance of the local fluctuating displacement field $u_i(\mathbf{x})$ (i is the Cartesian component), that describes the local deformation or dilation, $\langle [u_i(\mathbf{x})]^2 \rangle$ shows a *universal dependence* on the system size L as $[\ln(L/a_0)]^{2/3}$, a significantly weaker L-dependence than the well-known $\ln(L/a_0)$-dependence found away from T_c, or in one-component systems at any T; $a_0 = 2\pi/\Lambda$. Likewise, the two-point correlation function of the difference of the local displacements at two points separated by a distance r scales as $[\ln(r/a_0)]^{2/3}$, unlike the well-known $\ln(r/a_0)$-dependence of QLRO. These imply a positional order logarithmically stronger than the usual QLRO. We call this *positional SQLRO*, that forms an altogether *new, heretofore unstudied universality class*. The prediction of this SQLRO and the associated universality class is a principal outcome of the present study. The second-order transition remains unaffected with the critical exponents belonging to the Ising universality class, as they do in the corresponding rigid system. This is not the only state of the system near T_c. With sufficiently strong breaking of the Ising symmetry, the system distabilizes, leading to the loss of any SQLRO positional order (PO); only positional SRO is possible. This instability is driven by the selectivity parameters $\bar{g}_1$ and $\bar{g}_2$, which are also the Ising symmetry-breaking couplings. Our detailed results show that as the initial or microscopic value of the dimensionless ratio $\Gamma \equiv \bar{g}_1^2/(\mu g_1)$ exceeds a finite threshold Γ_{1c},

$$\frac{\bar{g}_1^2}{\mu g_1} > \Gamma_{1c} \approx 1.5, \quad (2)$$

the system destabilizes with the attendant loss of SQLRO. An analogous relation exists involving $\bar{g}_1, \tilde{\lambda}$, and g_2; see later. We further show that in such an elastic medium near T_c with Eq. (2) holding good, as soon as the system size L exceeds a threshold value L_c, controlled by the microscopic (bare) value of the selectivity parameters, is lost. Our theory gives the following expression of L_c:

$$L_c = a_0 \exp\left[\frac{\mu}{\left(\frac{\bar{g}_1^2}{2\mu} - g_1\right)} \frac{2\pi}{T_c} \right]. \quad (3)$$

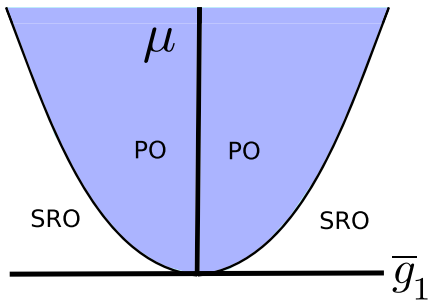

FIG. 1. Schematic phase diagram in the $\bar{g}_1$-μ plane for $d \geqslant 2$ near T_c. The blue shaded region is where $\mu > 0$ corresponding to positional SQLRO with second-order transition in 2D. The region outside has $\mu < 0$ implying loss of positional order or short-range order. The phase boundary (red) can be obtained by using Eq. (2) above (see text).

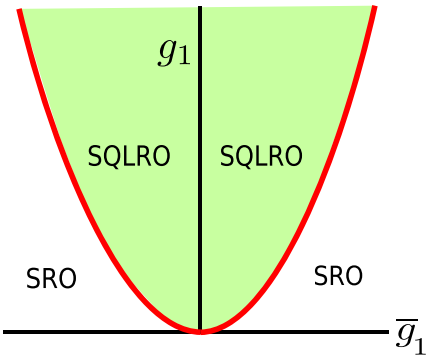

FIG. 2. Schematic phase diagram in the $\overline{g}_1$-g_1 plane for $d \geqslant 2$ near the phase transition. The middle light green region (PO), corresponds to SQLRO in 2D. The region outside has SRO. The phase boundary (red) can be obtained by using Eq. (2) above (see text).

Equation (2) allows us to draw the phase diagrams of the system in 2D, demarcating the phases with PO (i.e., SQLRO) and without PO (i.e., with SRO) which are shown in the schematic phase diagrams in Figs. 1–3. The $\overline{g}_1$ versus μ curve for a fixed g_1, and the $\overline{g}_1$ versus g_1 curve for a fixed μ, which are the phase boundaries between the ordered (PO) phase and disordered phase (SRO), are obviously parabolas as can be seen by equating $\overline{g}_1^2/(\mu g_1)$ with Γ_{1c}; see Eq. (2). Furthermore, a phase diagram can be drawn in $\overline{g}_1^2$-L plane showing the regions with PO and SRO by using Eq. (3); see Fig. 3.

Similar phase diagrams could be drawn in terms of $\overline{g}_2$ and g_2, $\tilde{\lambda}$, or L (not shown here).

The above results assumed a second-order transition of the order parameter field. However, the transition of the order parameter field too can depend very sensitively on the order parameter – strain couplings. While this is second order for weak order parameter-strain couplings, it can be turned first order by sufficiently strong order parameter – strain couplings. In the latter case, the system can still show positional order, which in this case would be just conventional QLRO, or can destabilize, and undergoes a transition to SRO for larger couplings. However, the distinctive feature of positional QLRO together with a first-order transition is that across the first-order transition temperature, there is a *finite jump* in the effective elastic modulii, unlike across second-order transitions. With a first-order transition, the instability in the positional order is, however, independent of the system size L, i.e., it sets in independent of the system size.

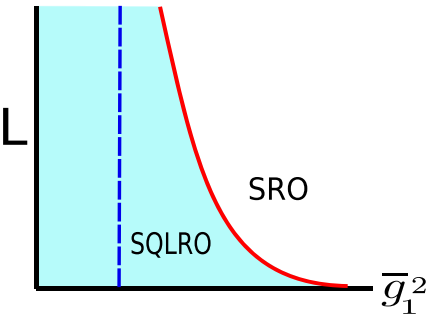

FIG. 3. Schematic phase diagram in the $\overline{g}_1^2 - L$ plane in 2D near T_c. The red curved line corresponding to $L = L_c$, the instability threshold, demarcates regions with PO (SQLRO) and SRO. The region left to the vertical broken blue line corresponds to systems with arbitrarily large L retaining PO. The region between the vertical blue line and the curved red line given by (3) corresponds to systems having a finite $L < L_c$, a threshold value maintaining PO and is identified with the persistence length or positional correlation length ξ; for $L > L_c = \xi$ only SRO is possible (see text).

B. Results on 3D systems

At 3D, for low selectivity, there are no infinite renormalizations of μ and $\tilde{\lambda}$; therefore, the displacement fluctuations show true positional LRO, indistinguishable from pure 3D elastic media. However, again a sufficiently strong selectivity, exceeding a dimension-dependent threshold, can distabilize the positional order. Unlike its 2D counterpart, this threshold is independent of L. In this case, the phase transition of the order parameter is unaffected by the order parameter-displacement couplings, and belongs to the 3D Ising universality class. Stronger selectivity parameters can introduce a first-order transition as well, in a way similar to the 2D case, with the elastic modulii displaying finite jumps across the first-order transition temperature. These results are shown in the schematic phase diagrams in Fig. 1 and Fig. 3.

These results including the phase diagrams could be verified in numerical simulations of the associated Ising spin-lattice discrete model close to the phase transitions. These may also be tested in carefully prepared purpose-built mixed ZTE samples (of magnetic or nonmagnetic origins), which undergo phase transitions within the temperature range of ZTE behavior, in future.

III. LANDAU-GINZBURG FREE ENERGY

We start by formulating the coarse-grained LG theory of a spin model for Ising transitions in a deformable ZTE. For simplicity, we schematically consider a conceptual model consisting of ferromagnetic Ising spins with nearest neighbor interactions on a Hookean spring-like model of isotropic gel. We assume the Hamiltonian $\mathcal{H}$:

$$\begin{aligned}\mathcal{H} = &-\sum_{\alpha\beta} J_{\alpha\beta}[(\mathbf{x}_\alpha - \mathbf{x}_\beta - \tilde{\mathbf{a}})^2]S_\alpha S_\beta \\ &+ \sum_{\alpha\beta} S_\alpha J'_{\alpha\beta}[(\mathbf{x}_\alpha - \mathbf{x}_\beta - \tilde{\mathbf{a}})^2] \\ &+ \frac{1}{2}\sum_{\alpha\beta} K_{\alpha\beta}(\mathbf{x}_\alpha - \mathbf{x}_\beta - \tilde{\mathbf{a}})^2. \end{aligned} \tag{4}$$

Here, α, β refer to lattice sites with position vectors $\mathbf{x}_\alpha$, $\mathbf{x}_\beta$, and not Cartesian components, and $S_\alpha = \pm 1$ is the Ising spin at lattice site α; all the sums over α, β are restricted to nearest neighbors. The constant $\tilde{a}$ is the rest length of the springs. Then in the rigid lattice limit of the lattice, $\mathbf{y} \equiv \mathbf{x}_\alpha - \mathbf{x}_\beta - \tilde{\mathbf{a}} = 0$, where y is a measure of the strain. Further, $J_{\alpha\beta}$ is the exchange integral that is assumed to depend quadratically on the strain for small strains: we assume $J_{\alpha\beta}(y) = J^0_{\alpha\beta} + J^1_{\alpha\beta}y^2$ for small y. Here, $J^0_{\alpha\beta} > 0$ is the exchange integral in the limit of an undistorted lattice. We further assume $J^1_{\alpha\beta} > 0$ for stability reasons. We have also included an Ising inversion

symmetry breaking term that is linear in S_α but quadratic in the strain, and is formally like a "local magnetic field"; $J'_{\alpha\beta}(y) = J'^{0}_{\alpha\beta} y^2$ for small y. Here, the coupling $J'_{\alpha\beta}$ can be of any sign. As mentioned earlier, such an Ising symmetry breaking coupling, although is not commonly considered in magnetic crystals, routinely appears in the free energies of two-component soft matter systems, where the Ising degree of freedom represents the local difference in the two components of a mixed system; see, e.g., Ref. [24]. In that spirit and to generalize our theory, we allow for such an anhamornic coupling in our model. Clearly, in the rigid limit of the lattice $J_{\alpha\beta}(y=0) = J^0_{\alpha\beta}$; $J'_{\alpha\beta}(y=0) = 0$, reducing $\mathcal{H}$ in Eq. (4) to the standard ferromagnetic Ising Hamiltonian [6]. Lastly, $K_{\alpha\beta}(\mathbf{x}_\alpha - \mathbf{x}_\beta - \tilde{\mathbf{a}})^2$, which is the last term in (4), gives the stretching energy of the Hookean springs. We now construct the LG free-energy functional for an isotropic system, assuming that in the rigid limit of the medium the phase transition is of continuous nature, described by a local scalar order parameter $\phi(\mathbf{x})$ representing the local Ising degree of freedom. As discussed above, in an actual physical realization of this model, ϕ could be a local magnetic (Ising-type) spin, or the local concentration difference of the two components that make up the elastic medium. The quadratic dependence of the interactions on the strains ensures ZTE here. We have ignored contributions anhamornic (i.e., non-Hookean) in the strain, since they turn out to be irrelevant in what follows below.

The Landau-Ginzburg free-energy functional $\mathcal{F}$ for this system is obtained by expanding in terms of the fields and their gradients, assuming small fluctuations [6]. For a two-component elastic medium, this should have three distinct parts:

$$\mathcal{F} = \mathcal{F}_\phi + \mathcal{F}_u + \mathcal{F}_{u\phi}. \tag{5}$$

For reasons of analytical manipulations (see later), we write down $\mathcal{F}$ in general d dimensions. Here, $\mathcal{F}_\phi$ is the free-energy functional of an isolated Ising model with all the displacements $u_i(\mathbf{x}) = 0$ (e.g., on a rigid lattice):

$$\mathcal{F}_\phi = \int d^d x \left[\frac{r}{2}\phi^2 + \frac{1}{2}(\nabla\phi)^2 + v\phi^4 \right]. \tag{6}$$

Here, $v > 0$ and $r = T - T_c^0$, where T is the temperature and T_c^0 is the mean-field critical temperature of the Ising model. Further, $\mathcal{F}_u$ is the elastic free energy of deformation of an isolated elastic medium, which due to the invariance of the system under any translation or rotation can depend on $\mathbf{u}(\mathbf{x})$ only through the strain tensor $u_{ij} = \frac{1}{2}(\nabla_i u_j + \nabla_j u_i + \nabla_i u_m \nabla_j u_m)$ [6]. Now, assuming isotropy $\mathcal{F}_u$ must have the form [25]

$$\mathcal{F}_u = \frac{1}{2}\int d^d x [2\mu u_{ij} u_{ij} + \lambda u_{ii}]. \tag{7}$$

Parameters μ and λ are the well-known Lamé coefficients for an elastic medium [6]. For an incompressible medium, λ diverges and $u_{ii} \to 0$.

Last, $\mathcal{F}_{u\phi}$ is the free energy of interactions between the local order parameter and the local strain. General symmetry considerations dictate the following form for $\mathcal{F}_{u\phi}$:

$$\mathcal{F}_{u\phi} = \int d^d x \left[g_1 \phi^2 u_{ij}^2 + \bar{g}_1 \phi u_{ij}^2 + g_{20}\phi^2 u_{ii}^2 + \bar{g}_{20}\phi u_{ii}^2 \right], \tag{8}$$

to the leading order in gradients and fields. The form of $\mathcal{F}_{u\phi}$ is chosen in such a way to ensure that it and also the total free energy $\mathcal{F}$ are *even* (quadratic) in the strain. The invariance of $\mathcal{F}$ under constant shifts of $\mathbf{u}$ ensures that there are no couplings of the form $\mathbf{u}\cdot\nabla\phi$ in $\mathcal{F}_{u\phi}$. The local stress field σ_{ij} is the thermodynamic conjugate of u_{ij} and is given by [6]

$$\sigma_{ij} = u_{ij}[2\mu + g_1\phi^2 + \bar{g}_1\phi] + u_{mm}\delta_{ij}[\tilde{\lambda} + g_{20}\phi^2 + \bar{g}_{20}\phi], \tag{9}$$

giving strain u_{ij} to vanish identically in the zero stress state with $\sigma_{ij} = 0$. Furthermore, $\mathcal{F}$ in Eq. (5) is constructed in a way such that the thermal average of the strain tensor, $\langle u_{ij}\rangle = 0$ identically in the absence of any externally applied stress, as it should be for ZTE materials.

Let us consider the different anharmonic terms included in $\mathcal{F}_{u\phi}$. The terms on the the right side of Eq. (8) may be interpreted as order parameter-dependent Lamé coefficients. In fact, by combining with Eq. (7), we may define effective or local Lamé coefficients

$$\mu(\phi) = \mu + g_1\phi^2 + \bar{g}_1\phi, \tag{10}$$

$$\lambda(\phi) = \lambda + 2g_{20}\phi^2 + 2\bar{g}_{20}\phi. \tag{11}$$

Thus, the effective Lamé coefficients depend on the local order parameter, not only through its magnitude, but also its sign, i.e., by the overall state of the local order parameter. These anhamornic terms may be alternatively interpreted as follows. The terms $[g_1(u_{ij})^2 + g_{20}(u_{ii})^2]\phi^2$ can be considered as the local strain-dependent corrections to T_c^0 giving T_c, the local effective critical temperature:

$$T_c = T_c^0 - 2[g_1(u_{ij})^2 + g_{20}(u_{ii})^2]. \tag{12}$$

Further, the terms $[\bar{g}_1(u_{ij})^2 + \bar{g}_{20}(u_{ii})^2]\phi$ together effectively act like a local aligning field term $h_\phi\phi$ in $\mathcal{F}$, where

$$h_\phi = -\left[\bar{g}_1(u_{ij})^2 + \bar{g}_{20}(u_{ii})^2\right], \tag{13}$$

that is the analog of an external conjugate field [26].

To generalize the scope of our study, we have included Ising $\mathcal{Z}_2$ symmetry breaking terms $\bar{g}_1\phi u_{ij}^2$ and $\bar{g}_{20}\phi u_{ii}^2$ in $\mathcal{F}_{u\phi}$ to allow for the possibility that the local strain couples with the two states of the Ising degree of freedom differently or *selectively*: the magnitudes of the parameters $\bar{g}_1$ and $\bar{g}_{20}$ thus give measures of the *degree of selectivity* in the model; these are also the parameters that introduce *inversion asymmetry* of the Ising order parameter [27]. This could be potentially important, e.g., in a two-component composite ZTE elastic medium, where the local elastic modulii may depend explicitly on the relative concentration of the two components. For instance, in a two-component binary mixture embedded in an elastic medium, the elastic deformations may couple selectively to the two local concentration of the two components [28,29]. These should result into the local elastic modulii depending asymmetrically upon the two states of the order parameter, e.g., relative concentration of the two components in a binary system, or both the sign and amplitude of the local order parameter. To generalize the scope of this study, we allow for such selectivity in composite ZTE elastic medium. These considerations motivate inclusion of the Ising $\mathcal{Z}_2$ symmetry breaking terms in $\mathcal{F}$, which leads to unexpectedly rich behavior [27]. These Ising-symmetry breaking terms

in Eq. (8) make it different from its counterparts used in Refs. [12,30] (studied in somewhat different contexts though). Couplings $v,\ g_1,\ g_2 > 0$ for thermodynamic stability, where as couplings $\bar{g}_{10},\ \bar{g}_2$ can be of either sign.

It is convenient to write the fields in the Fourier space as functions of the wave vector $\mathbf{q}$, and decompose $\mathbf{u}(\mathbf{q})$ as the vector sum of $\mathbf{u}^L(\mathbf{q})$ and $\mathbf{u}^T(\mathbf{q})$:

$$\mathbf{u}(\mathbf{q}) = \mathbf{u}^L(\mathbf{q}) + \mathbf{u}^T(\mathbf{q}), \tag{14}$$

where $\mathbf{u}^L(\mathbf{q})$ and $\mathbf{u}^T(\mathbf{q})$ are projections of $\mathbf{u}(\mathbf{q})$ along and perpendicular to the wave vector $\mathbf{q}$. Thus,

$$u_i^L(\mathbf{q}) = Q_{ij}(\mathbf{q})u_j(\mathbf{q}), \quad u_i^T(\mathbf{q}) = P_{ij}(\mathbf{q})u_j(\mathbf{q}), \tag{15}$$

where $Q_{ij}(\mathbf{q}) = q_i q_j/q^2$ is the longitudinal projection operator, and $P_{ij}(\mathbf{q}) = \delta_{ij} - q_i q_j/q^2$ is the transverse projection operator, which project, respectively, any vector onto the space parallel and perpendicular to $\mathbf{q}$. Free energy $\mathcal{F}$ can then take the form, after dropping cubic or higher-order terms in $\nabla_i u_j$ that are irrelevant in the renormalization group (RG) sense

$$\mathcal{F} = \int d^dx \Big[\frac{r}{2}\phi^2 + \frac{1}{2}(\nabla\phi)^2 + v\phi^4 + \mu\big(\nabla_i u_j^T\big)^2 + \frac{\tilde{\lambda}}{2}\big(\nabla_i u_j^L\big)^2 + (g_1\phi^2 + \bar{g}_1\phi)\big(\nabla_i u_j^T\big)^2 + (g_2\phi^2 + \bar{g}_2\phi)\big(\nabla_i u_j^L\big)^2\Big], \tag{16}$$

where $u_i^L(\mathbf{x})$ and $u_i^T(\mathbf{x})$ are the inverse Fourier transforms of $u_i^L(\mathbf{q})$ and $u_i^T(\mathbf{q})$; $\tilde{\lambda} = \lambda + 2\mu$, $g_2 = g_{20} + g_1$, $\bar{g}_2 = \bar{g}_1 + \bar{g}_{20}$. In Eq. (16), $\bar{g}_1$ and $\bar{g}_2$ are the selectivity parameters. The corresponding partition function is given by

$$\mathcal{Z} = \int \mathcal{D}\phi\mathcal{D}u_i^T\mathcal{D}u_i^L \exp(-\beta\mathcal{F}), \tag{17}$$

where $\beta \equiv 1/T$ with the Boltzmann constant $k_B = 1$. Dimensions and estimates for these parameters are available in Appendix B. It can be shown that with the form of $\mathcal{F}$ as given in Eq. (16), $dT_c/dV = 0$ [31]. Our theory differs from the one studied in Ref. [13] due to the presence of the spin-lattice anhamornic terms, which are irrelevant in the presence of a finite thermal expansion, and are not considered in Ref. [13]. We note that Eq. (16) does not contain any term that is odd in strain, for such a term would lead to $\langle u_{ij}\rangle \neq 0$, violating the condition of ZTE.

IV. GAUSSIAN THEORY

Ignoring the anharmonic terms, the free-energy Eq. (16) reduces to

$$\mathcal{F}_g = \frac{1}{2}\int \frac{d^dq}{(2\pi)^d}[(r+q^2)|\phi(\mathbf{q})|^2 + 2\mu|\mathbf{u}^T(\mathbf{q})|^2 + \tilde{\lambda}|\mathbf{u}^L(\mathbf{q})|^2]; \tag{18}$$

see Appendix C for more details. This gives for the displacement correlation functions at the harmonic order

$$\big\langle u_i^L(\mathbf{q})u_j^L(-\mathbf{q})\big\rangle = \frac{T\delta_{ij}}{\tilde{\lambda}q^2}, \tag{19}$$

$$\big\langle u_i^T(\mathbf{q})u_j^T(-\mathbf{q})\big\rangle = \frac{T\delta_{ij}}{2\mu q^2} \tag{20}$$

at all temperatures T. Equations (19) and (20) give

$$\big\langle\big(u_i^T\big)^2\big\rangle = \frac{T}{2\pi\tilde{\lambda}}\ln(L/a_0), \tag{21}$$

$$\big\langle\big(u_i^L\big)^2\big\rangle = \frac{T}{4\pi\mu}\ln(L/a_0) \tag{22}$$

in 2D. Similarly, the correlation functions of the elastic distortions are given by

$$C_{uu0}^T \equiv \langle[\mathbf{u}^T(\mathbf{x}) - \mathbf{u}^T(\mathbf{x}')]^2\rangle \approx \frac{T}{4\pi\mu}\ln(r/a_0), \tag{23}$$

$$C_{uu0}^L \equiv \langle[\mathbf{u}^L(\mathbf{x}) - \mathbf{u}^L(\mathbf{x}')]^2\rangle \approx \frac{T}{2\pi\tilde{\lambda}}\ln(r/a_0) \tag{24}$$

in the limit of large separation $r \equiv |\mathbf{x} - \mathbf{x}'|$ in 2D. Equations (21)–(24) correspond to positional quasi-long-range order (QLRO). At $d > 2$,

$$\big\langle\big(u_i^T\big)^2\big\rangle = \frac{T}{2\pi\tilde{\lambda}}\Lambda, \tag{25}$$

$$\big\langle\big(u_i^L\big)^2\big\rangle = \frac{T}{4\pi\mu}\Lambda, \tag{26}$$

which imply positional long-range order (LRO); where Λ is an upper wave-vector cutoff, $\Lambda = 2\pi/a_0$. From the free-energy Eq. (16) it is clear that the local order parameter $\phi(\mathbf{x})$ introduces corrections to the elastic modulii μ and λ; alternatively, the elastic distortions at different points in the system interact via the order parameter fluctuations. At any temperature away from T_c, the fluctuations of $\phi(\mathbf{x})$ are *short-ranged*, and hence, only short-ranged interactions between local displacement fields are generated. In contrast, near T_c, fluctuations of $\phi(\mathbf{x})$ are scale-invariant and *long-ranged*, leading to the local displacement fields interacting via effective *long-range* interactions. Interestingly, this takes the system potentially out of the jurisdiction of MWHT. Whether close to T_c these interactions lead to a phase that is *more ordered* or *less ordered* cannot however be inferred without detailed calculations. Below we calculate the precise quantitative system size dependence of $\langle(u_i^L)^2\rangle$ and $\langle(u_i^T)^2\rangle$, and the analogs of the correlation functions defined above in Eqs. (23) and (24), which should reveal the nature of order near T_c. Due to the large critical point fluctuations, naïve perturbation theory fails. To circumvent this problem, we resort to the perturbative RG framework that we discuss below.

V. ANHARMONIC THEORY

Anhamornic effects are likely to substantially alter the Gaussian theory results Eqs. (21), (22), (23), (24), (25) and (26) near the critical point. We discuss here in details the RG analysis, that we execute at the one-loop order, of the free-energy Eq. (16). By construction $\mathbf{u}^T \cdot \mathbf{u}^L = 0$. This allows us to mutually completely decouple the RG calculations for $\mu,\ g_1,\ \bar{g}_1$ and $\tilde{\lambda},\ g_2,\ \bar{g}_2$ at the one-loop order.

Before we embark on the RG calculations, we note that the anhamornic coupling constant v has $d_c = 4$ as the critical dimension, where as $d_c = 2$ for $g_1,\ \bar{g}_1,\ g_2$, and $\bar{g}_2$; see Appendix D 1. Since we will perform this RG in an expansion around the critical dimension $d_c = 2$, it is useful to consider $\mathcal{F}$

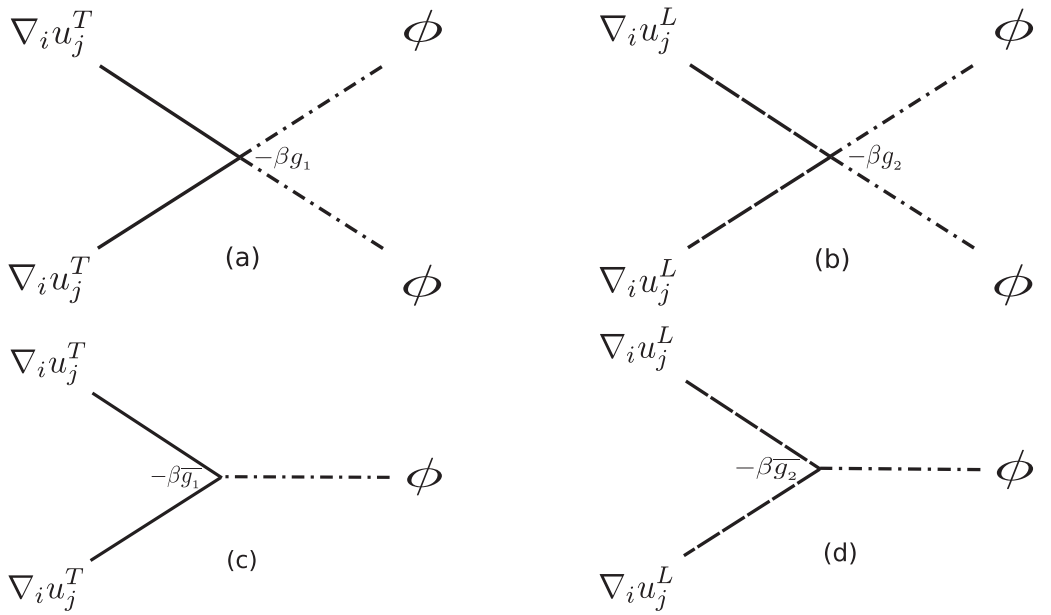

FIG. 4. Vertices for the Feynman graphs (a) $g_1\phi^2[\mathbf{u}^T(\mathbf{x})]^2$, (b) $g_2\phi^2[\mathbf{u}^L(\mathbf{x})]^2$, (c) $\bar{g}_1\phi[\mathbf{u}^T(\mathbf{x})]^2$, (d) $\bar{g}_2\phi[\mathbf{u}^L(\mathbf{x})]^2$.

to arbitrary d dimensions (see above), instead of considering specific physical dimensions of $d = 2, 3$.

Since the couplings g_1, $\bar{g}_1$, g_2, and $\bar{g}_2$ are irrelevant (in the RG sense) near $d_c = 4$, we can conclude that a second-order transition for the order parameter field ϕ at dimensions $4 \geqslant d \geqslant 2$, belongs to the Ising universality class [6], and is unaffected by the elastic deformations; see also Ref. [30] for similar discussions. That a second order transition is possible even in the presence of the inversion symmetry breaking terms in $\mathcal{F}$ [see Eq. (16)] can be argued in a manner that is exactly analogous to the existence of a second order liquid-gas transition; see Sec. VI for more details. Here, we assume the existence of a critical point and proceed to examine its consequence. It now remains to calculate how the order parameter fluctuations affect the lattice deformation fluctuations. As already explained, away from the critical point, effects of the ϕ-fluctuations are *small*, which leave the scaling of the variances $\langle[u_i^L(\mathbf{x})]^2\rangle$ and $\langle[u_i^T(\mathbf{x})]^2\rangle$ and the corresponding correlation functions unchanged from their forms in the harmonic theory, whereas close to the critical point, the observed scaling may change. Hence, below we focus only on the critical region and set $T = T_c$. Being closed to the critical point, we can then set up the renormalized perturbation theory solely for the displacement fields $\mathbf{u}(\mathbf{x})$ and expand in the powers of the coupling constants g_1, $\bar{g}_1$, g_2, $\bar{g}_2$ for a given configuration of ϕ, and subsequently averaging over the Boltzmann distribution of ϕ, controlled by $\mathcal{F}_\phi$ given above [30].

We employ the Wilson momentum shell procedure [2,6]. This method consists of tracing over the short wavelength Fourier modes of $\phi(\mathbf{x})$ and $u_i(\mathbf{x})$, followed by a rescaling of lengths. In particular, we follow the standard approach of initially restricting wave vectors to lie in a bounded spherical Brillouin zone: $|\mathbf{q}| < \Lambda$. The fields $\phi(\mathbf{x})$ and $u_i(\mathbf{x})$ are separated into high and low wave-vector parts $\phi(\mathbf{x}) = \phi^<(\mathbf{x}) + \phi^>(\mathbf{x})$ and $u_i(\mathbf{x}) = u_i^<(\mathbf{x}) + u_i^>(\mathbf{x})$ where $\phi^>(\mathbf{x})$ and $u_i^>(\mathbf{x})$ are nonzero only in the large-wave-vector (short wavelength) range $\Lambda e^{-dl} < |\mathbf{q}| < \Lambda$, while $\phi^<(\mathbf{x})$ and $u_i^<(\mathbf{x})$ have support in the small-wave-vector (long wavelength) range $|\mathbf{q}| < e^{-dl}\Lambda$. We then integrate out $\phi^>(\mathbf{x})$ and $u_i^>(\mathbf{x})$. This integration is done perturbatively in the anharmonic couplings g_1, $\bar{g}_1$, g_2, and $\bar{g}_2$ in Eq. (16); as usual, this perturbation theory can be represented by Feynman graphs, with the order of perturbation theory reflected by the number of loops in the graphs we consider. We confine our study to the one-loop renormalized theory here. The Feynman graphs or the vertices representing the anhamornic couplings $g_1\phi^2[\mathbf{u}^T(\mathbf{x})]^2$, $\bar{g}_1\phi[\mathbf{u}^T(\mathbf{x})]^2$, $g_2\phi^2[\mathbf{u}^L(\mathbf{x})]^2$, and $\bar{g}_2\phi[\mathbf{u}^L(\mathbf{x})]^2$ are illustrated in Fig. 4.

Next to the above perturbative step, we rescale lengths to restore the upper cut off back to Λ: $\mathbf{x} = \mathbf{x}'b$, $b = \exp(dl)$. We then rescale the long wavelength parts of the fields according to $u_i(\mathbf{x}) = \zeta_u u_i(\mathbf{x}')$ and $\phi(\mathbf{x}) = \zeta_\phi\phi(\mathbf{x}')$. We determine ζ_u by demanding that under the rescaling μ, $\tilde{\lambda}$ do not scale. This gives $\zeta_u = b^{1-d/2}$. We further determine ζ_ϕ by demanding that the coefficient of $\int d^dx(\nabla\phi)^2$ remains unity under rescaling. This gives $\zeta_\phi = b^{1-d/2}$; see Appendix D 1. We restrict ourselves to a one-loop calculation. At this order, both μ and $\tilde{\lambda}$ receive two fluctuation corrections each, originating from nonzero g_1, $\bar{g}_1$, g_2 and $\bar{g}_2$. The relevant Feynman diagrams for μ are given in Fig. 5. There are two similar Feynman diagrams that renormalize $\tilde{\lambda}$; they are discussed in Appendix D 2 (see Fig. 15).

Likewise coupling constants g_1, $\bar{g}_1$ are each renormalized at the one-loop order by the Feynman graphs illustrated in Figs. 6 and 7, respectively. Evaluation of these Feynman diagrams are discussed in more details in Appendix D 2. The corresponding Feynman graphs for g_2, $\bar{g}_2$ are given in Appendix D 2. As shown there, *all* the one-loop diagrams are proportional to $\langle\phi^>(\mathbf{x})^2(x)\rangle = \int_{\Lambda/b}^{\Lambda}\frac{d^dq}{(2\pi)^d}\langle|\phi(\mathbf{q})|^2\rangle$. We now use the well-known relation

$$\frac{\partial\langle\phi^2(\mathbf{x})\rangle}{\partial T} \sim -C_v, \tag{27}$$

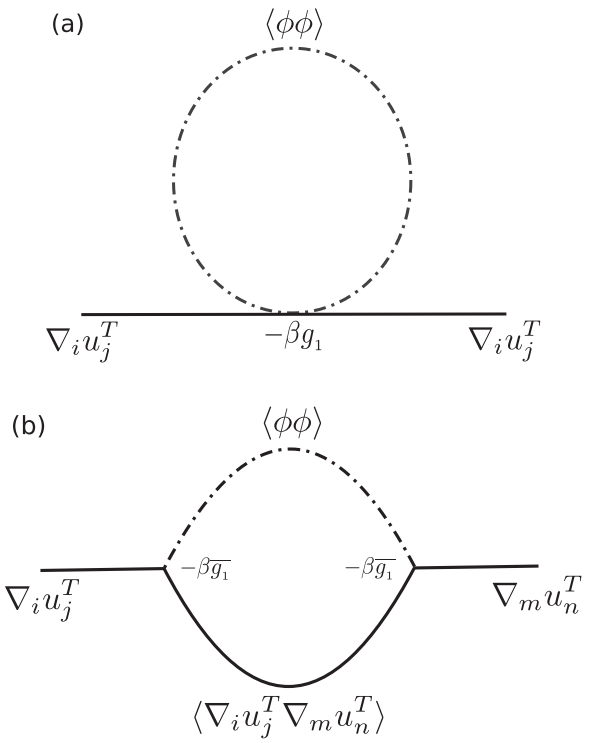

FIG. 5. One-loop diagrams that contribute to the fluctuation corrections of μ. Diagram (a) comes from the nonlinear coupling g_1, where as diagram (b) comes from $\bar{g}_1$ (see text).

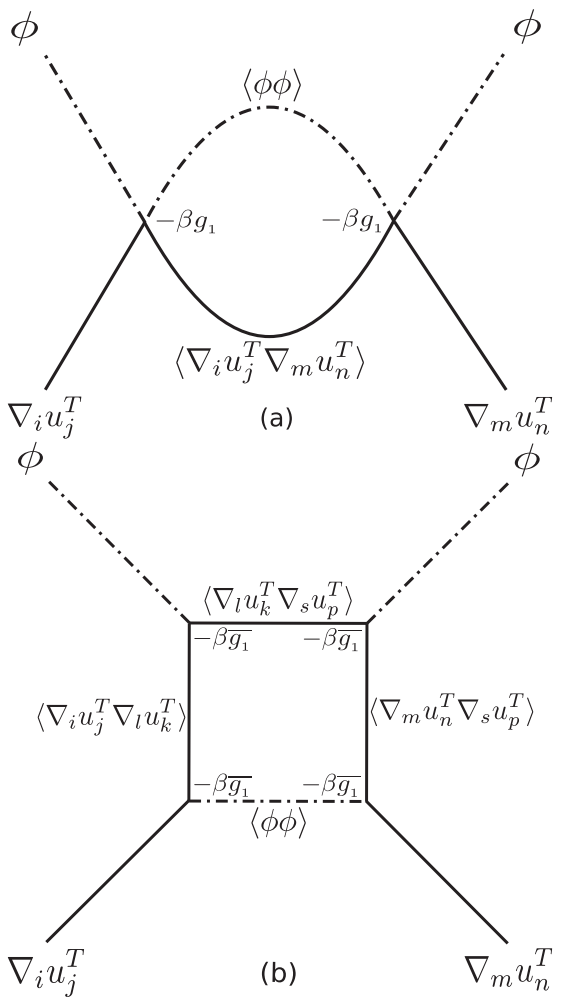

FIG. 6. One-loop diagrams that contribute to the fluctuation corrections of g_1. Diagram (a) depends only on g_1, whereas diagram (b) depends only on $\bar{g}_1$.

where C_v is the specific heat at constant volume [30]. As $T \to T_c$, $C_v \sim |T - T_c|^{-\alpha}$, where α is the specific heat exponent. At 2D, $\alpha = 0$ exactly [32], which corresponds to a logarithmic divergence in C_v as $T \to T_c$: $C_v \sim \ln(|T - T_c|/T_c)$. For $4 > d > 2$, α is nonzero, and not known exactly, but known perturbatively (or numerically, e.g., $\alpha = 0.11$ in 3D) [33], giving $C_v \sim |T - T_c|^{-\alpha}$. This gives at 2D,

$$\langle\phi^2(\mathbf{x})\rangle \sim \ln(|T - T_c|/T_c), \tag{28}$$

where as at higher dimensions,

$$\langle\phi^2(\mathbf{x})\rangle \sim |T - T_c|^{-\alpha+1}. \tag{29}$$

Now as $T \to T_c$, correlation length $\xi \sim |T - T_c|^{-\nu}$. The correlation length exponent $\nu = 1$ is again known exactly at 2D, or at higher dimension, ν is known perturbatively or numerically: $\nu \approx 0.63$ at 3D. This gives $\langle\phi^2(\mathbf{x})\rangle \approx T_c \ln\xi \times \mathcal{O}(1)$ at 2D, and $\langle\phi^2(\mathbf{x})\rangle \sim T_c\xi^{(-\alpha+1)/\nu}$. These are discussed in Appendix D 2. As already mentioned above, one-loop renormalization of μ, g_1, $\bar{g}_1$ are fully decoupled from those of $\tilde{\lambda}$, g_2, $\bar{g}_2$. The result is the following recursion relations

$$\frac{d\mu}{dl} = T_c g_1 - \frac{T_c\bar{g}_1^2}{2\mu}, \tag{30}$$

$$\frac{d\tilde{\lambda}}{dl} = 2T_c g_2 - \frac{2T_c\bar{g}_2^2}{\tilde{\lambda}}, \tag{31}$$

$$\frac{dg_1}{dl} = -\epsilon g_1 - \frac{2T_c g_1^2}{\mu} - \frac{T_c\bar{g}_1^4}{8\mu^3}, \tag{32}$$

$$\frac{d\bar{g}_1}{dl} = -\frac{\epsilon}{2}\bar{g}_1 + \frac{T_c\bar{g}_1^3}{2\mu^2} - \frac{2T_c g_1\bar{g}_1}{\mu}, \tag{33}$$

$$\frac{dg_2}{dl} = -\epsilon g_2 - \frac{4T_c g_2^2}{\tilde{\lambda}} - \frac{T_c\bar{g}_2^4}{\tilde{\lambda}^3}, \tag{34}$$

$$\frac{d\bar{g}_2}{dl} = -\frac{\epsilon}{2}\bar{g}_2 + \frac{2T_c\bar{g}_2^3}{\tilde{\lambda}^2} - \frac{4T_c g_2\bar{g}_2}{\tilde{\lambda}}, \tag{35}$$

where $\epsilon \equiv d - 2$. To proceed further, we define two dimensionless effective coupling constants

$$\alpha_1 \equiv \frac{T_c g_1 S_d}{(2\pi)^d\mu}\Lambda^\epsilon, \quad \beta_1 \equiv \frac{T_c\bar{g}_1^2 S_d}{(2\pi)^d\mu^2}\Lambda^\epsilon, \tag{36}$$

$$\alpha_2 \equiv \frac{T_c g_2 S_d}{(2\pi)^d\tilde{\lambda}}\Lambda^\epsilon, \quad \beta_2 \equiv \frac{T_c\bar{g}_2^2 S_d}{(2\pi)^d\tilde{\lambda}^2}\Lambda^\epsilon. \tag{37}$$

Here, S_d is the surface area of a d-dimensional sphere of unit radius. As we will see below, the one-loop perturbation theory that we set up here is actually an expansion in α_1, α_2, β_1, and β_2 up to the linear order.

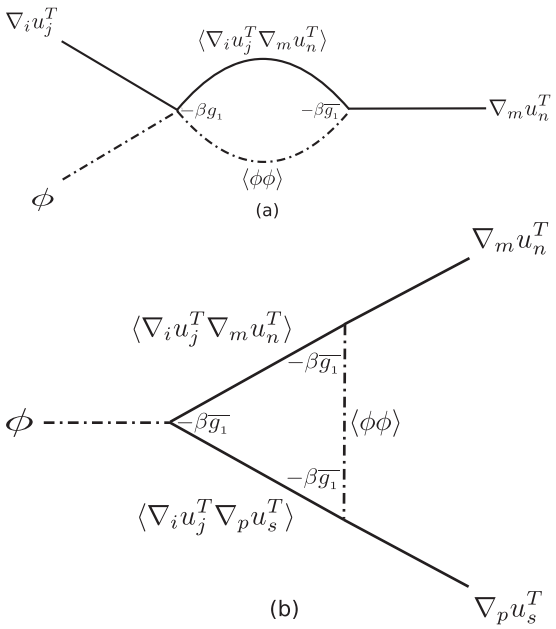

FIG. 7. One-loop diagrams that contribute to the fluctuation corrections of $\overline{g}_1$. Diagram (a) depends both g_1 and $\overline{g}_1$, whereas diagram (b) depends only on $\overline{g}_1$.

Next we obtain the RG recursion relations for $\alpha_1,\ \beta_1,\ \alpha_2,\ \beta_2$ by using the flow Eqs. (30)–(35):

$$\frac{d\alpha_1}{dl} = -\epsilon\alpha_1 - 3\alpha_1^2 - \frac{\beta_1^2}{8} + \frac{\alpha_1\beta_1}{2}, \tag{38}$$

$$\frac{d\beta_1}{dl} = -\epsilon\beta_1 + 2\beta_1^2 - 6\alpha_1\beta_1, \tag{39}$$

$$\frac{d\alpha_2}{dl} = -\epsilon\alpha_2 - 6\alpha_2^2 - \beta_2^2 + 2\alpha_2\beta_2, \tag{40}$$

$$\frac{d\beta_2}{dl} = -\epsilon\beta_2 + 8\beta_2^2 - 12\alpha_2\beta_2. \tag{41}$$

At 2D, we must set $\epsilon = 0$ in Eqs. (30)–(35) and (38)–(41).

A. Two-dimensional system: Thin elastic sheet

To study the system at 2D, we use the flow Eqs. (38)–(41) and set $\epsilon = 0$. Clearly, the only fixed points are $\alpha_1 = 0,\ \beta_1 = 0$ and $\alpha_2 = 0,\ \beta_2 = 0$. By exploiting the decoupling between $\mathbf{u}^T$ and $\mathbf{u}^L$, we separately focus on the phases and their stability in the $(\alpha_1,\ \beta_1)$ plane, which we work out in details below, and which suffices for incompressible systems. An identical analysis holds in the $(\alpha_2,\ \beta_2)$ plane.

Interestingly, the fixed point (0,0) is attractive (i.e., stable) along the α_1 direction, but repulsive (i.e., unstable) along the β_1 direction. Qualitatively thus, with a sufficiently large initial $\beta_1(l=0) \equiv \beta_{10} = T_c[\overline{g}_1(l=0)/\mu(l=0)]^2$ (i.e., β_{10} is the "bare" or unrenormalized value of β_1) much larger than the initial $\alpha_1(l=0) \equiv \alpha_{10} = T_c g_1(l=0)/\mu(l=0)$ (again, α_{10} is the "bare" or unrenormalized value of α_1), the system can become unstable, whereas a sufficiently small $\beta_{10} \ll \alpha_{10}$ may not be able to destroy the stable ordered phase observed for $\beta_1 = 0$. The question is, then where is the separatrix located in the α_1-β_1 plane, that separates the stable phase from the unstable phase? Since this putative separatrix must pass through the fixed point (0, 0), its general equation should be of the form $\beta_1 = \alpha_1 f(\alpha_1)$, with $f(\alpha_1) = \Gamma_1 +$ higher-order terms in α_1. Consistent with our lowest-order perturbation theory, we set $\beta_1 = \Gamma_1\alpha_1$ as the separatrix that passes through the origin and set out to calculate Γ_1. Flow Eqs. (38) and (39) may be written as

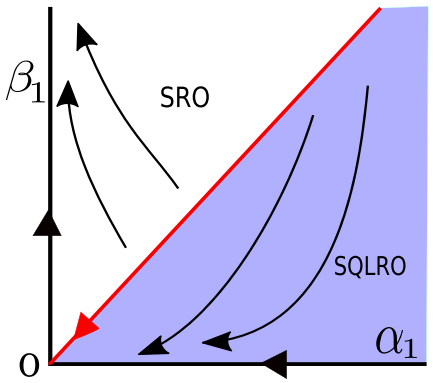

FIG. 8. RG flow diagram in the α_1-β_1 plane in 2D. The origin O is the only fixed point. The red line is the separatrix given by Eq. (46). Arrows indicate the flow directions (see text).

$$\frac{d\ln\alpha_1}{dl} = \alpha_1\left(-3 - \frac{\Gamma_1^2}{8} + \frac{\Gamma_1}{2}\right), \tag{42}$$

$$\frac{d\ln\beta_1}{dl} = \alpha_1(2\Gamma_1 - 6). \tag{43}$$

Thus,

$$\frac{d}{dl}\ln\Gamma_1 = \frac{d}{dl}\ln\beta_1 - \frac{d}{dl}\ln\alpha_1 = \alpha_1\left(\frac{3\Gamma_1}{2} - 3 + \frac{\Gamma_1^2}{8}\right) = 0, \tag{44}$$

giving the threshold Γ_{1c} as

$$\Gamma_{1c} = \tfrac{1}{2}[-12 + \sqrt{240}]. \tag{45}$$

Thus, if

$$\beta_1 = \Gamma_{1c}\alpha_1 = \tfrac{1}{2}[-12 + \sqrt{240}]\alpha_1, \tag{46}$$

equivalently,

$$\frac{\overline{g}_1^2}{\mu g_1} = \Gamma_{1c} \approx 1.5, \tag{47}$$

initially, this will continue to hold under renormalization. Points below this locus necessarily flow to the origin, where as points above this locus do not. They flow *away* from the origin, until they leave the regime of validity of our perturbation theory. See Fig. 8 for a schematic flow diagram.

The plot of Eq. (47) in the $\overline{g}_1$-μ for a fixed g_1 gives the phase diagram Eq. (1). Similarly, the plot of Eq. (47) in the $\overline{g}_1$-g_1 plane gives the phase diagram Eq. (2).

Let us first focus on the scaling properties when $\alpha_{10},\ \beta_{10}$, the initial values of the $\alpha_1,\ \beta_1$, lie *below* the separatrix. While all points below the line Eq. (46) eventually flow to the origin, we still need to find out the manner in which these points may approach the origin. That is to say, an arbitrary point

$[\alpha_1(l),\ \beta_1(l)]$ below Eq. (46) may, during its approach to the origin, either *go away* from Eq. (46), or *move toward* it, depending upon whether the locus Eq. (46) is *attractive* or *repulsive*. To know that let us assume $\beta_{10} = \Gamma(l=0)\,\alpha_{10}$, with $\Gamma_1(l=0) = \Gamma_{1c} - \delta_1(l=0)$, where small $\delta_1(l=0) > 0$ corresponding to an initial point below the separatrix Eq. (46). Therefore,

$$\begin{aligned}\frac{d}{dl}\ln\Gamma_1(l) &= \frac{1}{\Gamma_1}\frac{d\Gamma_1}{dl} = -\Gamma_{1c}\frac{d\delta_1}{dl}\\ &= -\alpha_1\left(\frac{\Gamma_{1c}^2}{8} - \frac{5\delta_1}{4} + \Gamma_{1c} - 3\right)\\ &= -\alpha_1\frac{\delta_1}{4}(\Gamma_{1c}+6) < 0,\end{aligned} \tag{48}$$

to the leading order in small δ_1. Equation (48) implies that $\delta_1(l)$ rises, or equivalently, $\Gamma_1(l)$ decreases as the renormalization group "time" l increases, corresponding to a *repulsive* separatrix. This further means

$$\frac{d}{dl}\ln\Gamma_1 = \frac{1}{\Gamma_{1c}}\frac{d}{dl}\left(\frac{\beta_1}{\alpha_1}\right) < 0. \tag{49}$$

Therefore, a point $(\alpha_1,\ \beta_1)$ that is slightly away from the separatrix Eq. (8) and lies on the stable side of it, not only flow toward the origin, it does so by *moving away* from the separatrix as the RG time l increases. We thus conclude that in the long wavelength limit, $\beta_1(l) \ll \alpha_1(l)$, $l \to \infty$. In this limit, then by using Eq. (38), we find

$$\frac{d\alpha_1}{dl} = -3\alpha_1^2, \tag{50}$$

giving

$$\frac{-1}{\alpha_1} = -3l - \frac{1}{\alpha_{10}} \approx -3l, \tag{51}$$

for large l, where α_{10}, a constant of integration, is the "initial value" of $\alpha_1(l)$. Therefore,

$$\alpha_1(l) = \frac{1}{3l} = \frac{T_c g_1(l)}{\mu(l)} \tag{52}$$

for large l. Likewise, we can find out $\beta_1(l)$ from Eq. (39). Using $\beta_1(l) \ll \alpha_1(l)$ in the long wavelength limit, Eq. (39) gives

$$\frac{d\beta_1}{dl} = -6\alpha_1\beta_1 = -\frac{2}{l}\beta_1. \tag{53}$$

This gives

$$\beta_1(l) \sim \frac{1}{l^2} \ll \alpha_1(l) \sim \frac{1}{l}, \tag{54}$$

which provides *aposteriori* justification of $\beta_1(l) \ll \alpha_1(l)$ that we have claimed above. We now calculate the renormalized shear modulus in the long wavelength limit. Using Eq. (30) together with Eq. (52) above and using $\beta_1(l) \ll \alpha_1(l)$,

$$\frac{d\mu}{dl} = \frac{\mu}{3l}, \tag{55}$$

in the limit of large l, which upon integration gives for the scale-dependent, renormalized, scale-dependent shear modulus $\mu(q)$,

$$\mu(q) \approx \mu_R[\ln(\Lambda/q)]^{1/3}, \tag{56}$$

for small enough q, where we have used $\ell = \ln b = \ln(\Lambda/q)$. Thus, $\mu(q)$ clearly diverges in the long wavelength limit $q \to 0$. Here, μ_R, a constant of integration, is the amplitude of the scale-dependent, renormalized shear modulus. Equation (56) is the analog of anomalous elasticity in 3D equilibrium smectics [23]. Thus,

$$\langle|\mathbf{u}^T(\mathbf{q})|^2\rangle \approx \frac{T_c}{2\mu_R|\ln(\Lambda/q)|^{1/3}q^2}, \tag{57}$$

for sufficiently small q. Equation (56) shows anomalous elasticity that arises due to the coupling with the critical order parameter, and illustrates the new universality class. What is the range of wave vectors over which Eq. (57) is valid? While the Landau-Ginzburg free-energy Eq. (16) is valid for wave vector $q \leqslant \Lambda$, the upper wave-vector limit of the validity of the corresponding renormalized free energy [and hence the correlation function Eq. (57)], which is $\tilde{\Lambda}$ must be *smaller* than Λ, for high wave vectors close to Λ, effects of renormalization would be small, and the harmonic theory should suffice there. Enough RG "time" l must be spent in order for the fluctuation effects to become dominant, to acquire substantial renormalization of the harmonic theory scaling. Equivalently, one might ask how big the system must be for it to display Eq. (57)? An estimate of that crossover scale ξ_{NL} may be obtained from Eq. (51) by noting that the "crossover RG time" l_{NL}, at which the anharmonic effects become substantial, is given by the condition $3l_{NL} \sim 1/\alpha_{10}$. This gives

$$\Lambda\xi_{NL} \approx \exp[\mu/(3g_1T_c)] \times \mathcal{O}(1). \tag{58}$$

Thus, ξ_{NL} that sets the scale at which anhamornic effects become important, depends sensitively on the model parameters and also T_c. For instance, if we consider two systems having same values for the model parameters, but their respective T_c's differing by a factor of 2, ξ_{NL} will differ by a factor of $e^2 \approx 7.4$. In fact, if the system size $L < \xi_{NL}$, the system does not get enough "renormalization group" time l to have substantial renormalization of the model parameters; as a result conventional QLRO ensues. However, for $L > \xi_{NL}$, the system gets enough RG time for substantial renormalization of the model parameters, and hence SQLRO follows.

We now calculate the variance $\langle[\mathbf{u}^T(\mathbf{x})]^2\rangle$ near $T = T_c$ that involves inverse Fourier transform of $\langle|\mathbf{u}^T(\mathbf{q})|^2\rangle$. Inverse Fourier transform of Eq. (57) gives

$$\begin{aligned}\langle[\mathbf{u}^T(\mathbf{x})]^2\rangle &= \int_{2\pi/L}^{\tilde{\Lambda}}\frac{d^2q}{(2\pi)^2}\langle|\mathbf{u}^T(\mathbf{q})|^2\rangle\\ &\approx \frac{T_c}{2\mu_R}\int_{2\pi/L}^{\tilde{\Lambda}}\frac{d^2q}{(2\pi)^2}\frac{1}{[q^2\{\ln(\Lambda/q)\}^{1/3}]}\\ &\approx \frac{3T_c}{8\pi\mu_R}[\ln(L/a_0)]^{2/3},\end{aligned} \tag{59}$$

in the limit of large L. This though rises with L and eventually diverges in the thermodynamic limit, it does so significantly more slowly than the QLRO, indicating an order *stronger* than QLRO. Henceforth, we call it SQLRO. In Eq. (59) above,

$\tilde{\Lambda}$ is an upper momentum cut off below which (i.e., $q < \tilde{\Lambda}$) Eq. (56) holds; see also Appendix D 3.

We next calculate the renormalized equal-time correlation function $C_{TT}(|\mathbf{x}-\mathbf{x}'|)$ of $\mathbf{u}^T(\mathbf{x})$ near $T = T_c$. We get

$$\begin{aligned} C_{TT}&(|\mathbf{x}-\mathbf{x}'|) \\ &\equiv \left\langle \left[u_i^T(\mathbf{x}) - u_i^T(\mathbf{x})\right]^2 \right\rangle \\ &\approx \int_0^{\tilde{\Lambda}} \frac{d^2k}{(2\pi)^2} \frac{T_c}{2\mu_R k^2 [\ln(\Lambda/k)]^{2/3}} \{1 - \exp[i\mathbf{k}\cdot(\mathbf{x}-\mathbf{x}')]\} \\ &\approx \frac{T_c}{4\pi\mu_R} [\ln|\mathbf{x}-\mathbf{x}'|\tilde{\Lambda}|]^{2/3}, \end{aligned} \tag{60}$$

in the limit of large $|\mathbf{x}-\mathbf{x}'|$. See details in Appendix D 4. Equations (59) and (60) are the essence of SQLRO, as already mentioned above; the alert reader will find them in Introduction above. Equations (59) and (60) define the new universality class close to second-order phase transitions of incompressible systems.

This is to be contrasted with the corresponding result for the displacement correlator $C^0_{TT}(|\mathbf{x}-\mathbf{x}'|)$ in the harmonic theory, where the same correlation function scales as $\ln(|\mathbf{x}-\mathbf{x}'|\Lambda)$. Thus, for large $|\mathbf{x}-\mathbf{x}'|$,

$$C_{TT}(|\mathbf{x}-\mathbf{x}'|) \ll C^0_{TT}(|\mathbf{x}-\mathbf{x}'|), \tag{61}$$

showing SQLRO as a distinctly stronger order than the well-known QLRO.

Let us consider the physics on the other side of, i.e., *above* the separatrix Eq. (46). The RG trajectories starting with initial values lying above the separatrix, but not far from the origin (to stay within the validity regime of our one-loop RG, at least for small α_{10}, β_{10}) flow away, since α_1 still flows to zero, whereas β_1 flows away, giving $\beta_1(l) \gg \alpha_1(l)$, which we show *a posteriori*. This follows directly from Eq. (48) with the replacement of δ_1 by $-\delta_1$ corresponding to an "initial condition" above the separatrix. It then follows

$$\frac{d}{dl}\ln\Gamma_1(l) = \frac{1}{\Gamma_{1c}}\frac{d}{dl}\left(\frac{\beta_1(l)}{\alpha_1(l)}\right) > 0, \tag{62}$$

meaning that starting from an initial condition that lies slightly above the separatrix, the RG trajectories will move toward to the origin along the α_1 direction but move away from it along the β_1 direction; see the flow lines in the flow diagram Eq. (8). It is useful to find out *how* $\beta_1(l)$ grows and $\alpha_1(l)$ decays in the limit of large l. It should be kept in mind though that on the unstable side of the separatrix, the accuracy of our one-loop RG gets progressively poorer with larger RG time l, since as l gets larger, $\beta_1(l)$ gets larger as well, eventually making the perturbative approximation untenable. Retaining the most dominant terms for large l, we find from Eq. (39)

$$\frac{d\beta_1(l)}{dl} = 2\beta_1^2, \tag{63}$$

giving

$$\beta_1(l) = \frac{\beta_{10}}{1 - 2l\beta_{10}}, \tag{64}$$

where $\beta_{10} = \beta_1(l=0)$ appears as a constant of integration. Thus, as $\beta_1(l)$ diverges as $l \to \ell_\beta \equiv 1/(2\beta_{10})$ from below, i.e., as the system size exceeds an initial condition-dependent finite size $L_\beta = a_0 \exp[1/(2\beta_{10})]$, a finite, model parameter-dependent nonuniversal size, from below. Similarly, retaining the most dominant terms we find from Eq. (38) for large l

$$\frac{d\alpha_1}{dl} = -\frac{\beta_1^2}{8} = \frac{-1}{8}\frac{\beta_0^2}{(1-2l\beta_0)^2}. \tag{65}$$

Thus, $\alpha_1(l)$ decreases monotonically as l increases. Solving, we find

$$\alpha_1(l) = c_\alpha + \frac{1}{32}\frac{1}{l - 1/(2\beta_{10})}. \tag{66}$$

Here, c_α is a constant of integration that can be fixed by demanding that at $l = 0$, $\alpha_1(l=0) = \alpha_{10} \equiv T_c g_1(l=0)/\mu(l=0)$, the "initial" or unrenormalized value of α_1. This gives $c_\alpha = \beta_{10}/16 + \alpha_{10}$, yielding

$$\alpha_1(l) = \frac{-1}{32}\frac{1}{1/(2\beta_{10}) - l} + \frac{\beta_{10}}{16} + \alpha_{10}. \tag{67}$$

Thus, $\alpha_1(l)$ continuously decreases as l increases, and eventually *vanishes* as the system size crosses a finite threshold $\tilde{\ell}$. This scale $\tilde{\ell}$ may be found by setting $\alpha(\tilde{\ell}) = 0$ giving

$$\tilde{\ell} = \frac{8\alpha_{10}}{\beta_{10}(\beta_{10} + 16\alpha_{10})} < \ell_\beta, \tag{68}$$

which unsurprisingly is finite and *nonuniversal*.

We now study the fate of $\mu(l)$ on this unstable side. In the limit $l \gg 1$, we get from Eq. (30)

$$\frac{d\mu}{dl} = -\mu\frac{\beta_1}{2} = -\frac{\mu\beta_{10}}{2(1/(2\beta_{10}) - l)}, \tag{69}$$

giving

$$\mu(l) = \tilde{\mu}_0 |\frac{1}{2\beta_{10}} - l|^{1/4}, \tag{70}$$

as $l \to \ell_\beta$ from below, where $\tilde{\mu}_0$ is a constant of integration: $\tilde{\mu}_0 = \mu(l=0)(\frac{1}{2\beta_{10}})^{1/4}$. Thus, $\mu(l)$ depends sensitively on β_{10}, and as $l \to \ell_\beta$ from below, $\mu(l)$ vanishes. Of course, we cannot follow $\mu(l)$ all the way to $l \to 1/(2\beta_{10})$ from below, as precisely there $\beta_1(l)$ diverges.

It is clear from the discussions above that for the stability of the system, RG "time" l should satisfy

$$l < \ell_c = l_\beta \equiv \frac{1}{2\beta_{10}} = \frac{1}{2}\frac{\mu^2(l=0)}{T_c \bar{g}_{10}^2(l=0)}, \tag{71}$$

whereas if $l > \ell_c$, then the system becomes unstable. Equivalently, the length scale for stability L_c, which is a measure of the positional correlation length, is given by

$$L_c = L_\beta = a_0 \exp\left[\frac{1}{2T_c}\frac{\mu^2(l=0)}{\bar{g}_{10}^2(l=0)}\right], \tag{72}$$

such that for system size $L < (>) L_c$, the system is stable and the system remains positionally ordered (unstable without any positional order). For a fixed L_c, this relation may be written in an alternative form:

$$\mu(l=0) = |\bar{g}_1(l=0)|\sqrt{T_c \ln(L_c/a_0)} \times \mathcal{O}(1). \tag{73}$$

Thus, L_c depends very sensitively on $\bar{g}_{10}$. For small g_{10}, L_c becomes very large. Readers who are interested in a perturbation theory argument for divergence of L_c for small $\bar{g}_1(l=0)$ can

find one in Appendix E. The interpretation of the separatrix as the threshold for breakdown of positional order is in fact supported from the fact that on the unstable side of the separatrix, an arbitrarily large system will not be able to sustain any positional order.

The instability discussed above occurs if

$$\Gamma_1(l=0) > \Gamma_{1c} = \frac{1}{2}[-12+\sqrt{240}], \tag{74}$$

or equivalently, the bare or unrenormalized model parameters satisfy

$$\frac{\overline{g}_1^2(l=0)}{\mu(l=0)g_1(l=0)} > \Gamma_{1c}. \tag{75}$$

In the unstable region of the parameter space, the elastic sheet can remain stable if it is sufficiently small, for in that case, $\mu(l=\ell_c)>0$, stabilizing the positional order. So long as the system size $L < L_c = a_0\exp(\ell_c)$, the positional order is stable since $\mu(l \lesssim \ell_c)$ remains positive. On the unstable side of the separatrix, starting from small "initial" values of α_1 and β_1, anharmonic effects will not be visible until $\beta_1(l=\ell^*) \sim \mathcal{O}(1)$. For $l < \ell^*$, the system remains stable and shows scaling as given by the Gaussian theory. Using Eq. (64), we get an estimate about ℓ^*:

$$\ell^* = \frac{1-\beta_{10}}{\beta_{10}} \times \mathcal{O}(1). \tag{76}$$

For $l \ll \ell^*$, there is no substantial renormalization of μ, and hence, the variance $\langle[\mathbf{u}^T(\mathbf{x})]^2\rangle$ should scale as $\ln(L/a_0)$, implying conventional QLRO.

The flow along the separatrix can be calculated. We find on the separatrix

$$\frac{d\alpha_1}{dl} = \alpha_1^2\left(-3-\frac{\Gamma_{1c}^2}{8}+\frac{\Gamma_{1c}}{2}\right) < 0, \tag{77}$$

$$\frac{d\beta_1}{dl} = 2\alpha_1\beta_1(\Gamma_{1c}-3) < 0, \tag{78}$$

implying a flow *toward* the origin.

Let us further analyze the behavior of the system qualitatively on the unstable side of the separatrix Eq. (46), where the RG trajectories flow out, eventually going out of the regime of validity of our perturbation theory. The system will then behave differently than what it does below the separatrix, i.e., in the stable regime. What might this different behavior be? Since the flows in this regime lead out of the region of validity of our perturbation theory, we cannot follow these flow lines, but can only speculate about it. For this, we are guided by the expectation that for large enough α_1 (which can be accessed by, e.g., high enough $T = T_c$), there should be a phase where positional order breaks down giving way to a "new phase" that only has short-range order. Accordingly, there must be an unstable critical point on the α_1 axis, controlling this transition to this putative phase. If we now consider the full RG flows for an elastic sheet near a second-order phase transition in the two dimensional parameter space (α_1, β_1) and connect this putative flow on the α_1 axis with our flows near the origin in the simplest possible way (i.e., one that does not involve introducing any other new fixed points), then we are then led to Fig. 9. This is essentially an "Occam's razor"-style argument: Fig. 9 has the simplest flow topology that naturally reduces to the known flow trajectories for small α_1, β_1 (as shown in Fig. 8). It at the same time gives the putative global flow allowing for a continuous transition to a phase with breakdown of positional order with breakdown of elasticity that we are tempted to identify with the liquidlike phase with SRO, where obviously the mean square displacement is unbounded. It for instance suggests that starting very close to this "conjectured unstable fixed point" on the α_1 axis, but outside of the separatrix (i.e., in the unstable region), we expect the resulting RG trajectories to follow the separatrix for a long "RG time," eventually moving away from it to flow away toward unbounded β_1 for large l. In 2D, this melting transition could be a first or second order. What if the putative transition to this phase is first order in nature? In that case, the conjectured unstable fixed point or the critical point with, e.g., a diverging correlation length and a continuously vanishing order parameter cannot exist. Still there should be a phase boundary schematically similar to that drawn in Fig. 9 that should presumably be a first-order boundary between a phase characterized by positional order and a new phase with only short-range order. In an RG description, the separatrix should still end at a critical point of certain type, where the associated exponents are such that they represent, for instance, a jump in the order parameter (e.g., a vanishing order parameter exponent in the ordered phase). While the true nature of the transition may still be somewhat unclear till the date, we expect the topology of the RG flow lines to remain the same regardless of the precise nature of the transition, and hence, we speculate Fig. 9 to hold in general.

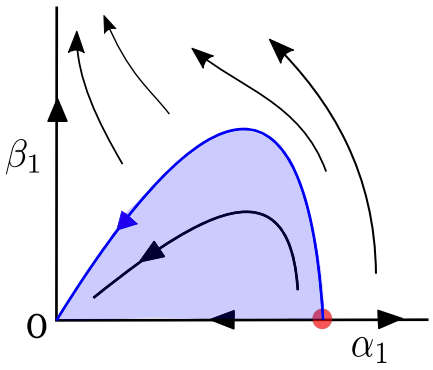

FIG. 9. Conjectured "Occam's razor" global RG flows in the α_1-β_1 plane at 2D. Arrows indicate the flow directions. The (light blue) shaded region is the stable region with positional SQLRO. The red circle on the α_1 axis is the putative unstable critical point not accessible in our perturbative RG (see text).

For nearly incompressible systems, $\tilde{\lambda} \to \infty$, and $u_{ii} \approx 0$. However, for compressible systems with vanishing strain in the zero-stress states, an identical analysis holds for the renormalization and scaling of the longitudinal displacements $\mathbf{u}^L(\mathbf{x})$. In summary: We again have (0,0) as the only fixed point in the α_2-β_2 plane, which is attractive along the α_2 axis and repulsive along the β_2 axis. Similar to the separatrix in the α_1-β_1 plane, there is a separatrix in the α_2-β_2 plane, such that for initial conditions lying below the separatrix, the RG flow is toward the origin, where as for initial conditions lying above the separatrix, the flow lines go away from the origin and eventually go out of the validity of the perturbation theory. The equation of the separatrix in the (α_2, β_2) plane, that is the

direct analog of Eq. (8) in the $(\alpha_1,\ \beta_1)$, is given by

$$\Gamma_{2c} = \tfrac{1}{2}[-6 \pm \sqrt{60}], \tag{79}$$

that is the analog of Γ_{1c} in Eq. (45). Proceeding as for $\mathbf{u}^T$, on the stable side of the separatrix, we find that

$$\frac{d\tilde{\lambda}}{dl} = 2g_2 = \frac{\tilde{\lambda}}{3l}, \tag{80}$$

giving for the scale-dependent, renormalized $\tilde{\lambda}(q)$ as

$$\tilde{\lambda}(q) = \tilde{\lambda}_R\left[\ln\left(\frac{\Lambda}{q}\right)\right]^{1/3}, \tag{81}$$

where $\tilde{\lambda}_R$ is the amplitude of renormalized bulk modulus. This in turn gives

$$\langle[\mathbf{u}^L(\mathbf{x})]^2\rangle \approx \frac{T_c}{2\pi\tilde{\lambda}_R}[\ln(L/a_0)]^{2/3}, \tag{82}$$

that is identical with the corresponding result for $\langle(\mathbf{u}^L(\mathbf{x}))^2\rangle$. Unsurprisingly, renormalized correlator $C_{LL}(|\mathbf{x}-\mathbf{x}'|) \equiv \langle[u_i^L(\mathbf{x}) - u_i^L(\mathbf{x}')]^2\rangle$ scales as $(T_c/\tilde{\lambda}_R)[\ln(|\mathbf{x}-\mathbf{x}'|)\tilde{\Lambda}]^{2/3}$ for large $|\mathbf{x}-\mathbf{x}'|$; here, $\tilde{\lambda}_R$ is the amplitude of the scale-dependent, renormalized shear modulus. This together with Eq. (82) are analogs of Eqs. (60) and (59). These four results establish the new universality class with SQLRO near T_c for second-order phase transitions in compressible elastic media.

A RG flow diagram analogous to Eq. (8) may be drawn in the α_2-β_2 plane; we do not show it here.

For initial conditions

$$\bar{g}_2^2(l=0)/[\tilde{\lambda}(l=0)g_2(l=0)] < (>)\Gamma_{2c} \equiv \tfrac{1}{2}[-6+\sqrt{60}], \tag{83}$$

the RG flow lines in the α_2-β_2 plane flow to (away from) the origin, with β_2 eventually diverging at a finite l and α_2 vanishing in the latter case.

It is possible that the initial conditions are such that $\Gamma_1 < (>)\Gamma_{1c}$ and $\Gamma_2 > (<)\Gamma_{2c}$, since all the phenomenological parameters are free parameters in our theory. In that case, $\mu(l)$ will stiffen (soften) and $\tilde{\lambda}(l)$ will soften (stiffen) due to the order parameter fluctuations near the critical point. Therefore, the longitudinal modes will have enhanced (reduced) fluctuations, whereas the fluctuations of the transverse modes will be suppressed (enhanced) due to the anhamornic effects. Thus, separate measurements of the longitudinal and transverse modes fluctuations should reveal important information about the microscopic parameters of the system. It should however be remembered as the fluctuations of either the longitudinal or transverse modes rise (being on the unstable side of the respective sepatarrix), eventually the anhamornic terms neglected in the strain (on the ground of being RG irrelevant) are going to be important, ultimately leading to disorder and overall loss of positional order for a sufficiently large system size L. We do not discuss that further here.

B. Bulk sample: $d > 2$

We now study the universal scaling properties at higher dimensions, i.e., $d = 2+\epsilon > 2$ near $T = T_c$. We use the flow

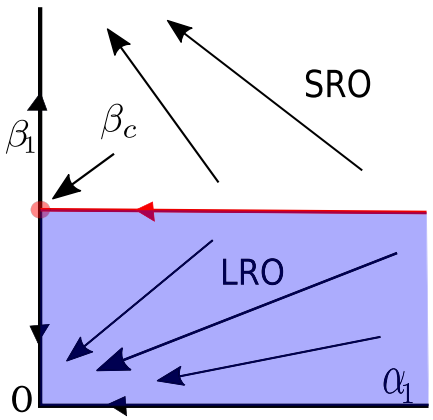

FIG. 10. RG flow diagram in the α_1-β_1 plane in 3D. The blue line is the separatrix given by $\beta = \epsilon/2$. The small circle on the β_1 axis is the unstable fixed point $(0,\ \beta_c)$. Arrows indicate the flow directions (see text).

Eqs. (38)–(41). There are now two fixed points for the RG flow Eqs. (38) and (39). These are (0,0) which is linearly stable and $(0,\ \epsilon/2)$ which is linearly stable along the α_1 direction, but unstable along β_1 direction. There could in principle be a third possibility of a fixed point, in which $\alpha_1 \neq 0$, and we solve

$$2\beta_1 - 6\alpha_1 = \epsilon, \tag{84}$$

$$-3\alpha_1^2 - \frac{\beta_1^2}{8} + \frac{\alpha_1\beta_1}{2} = \epsilon\alpha_1 \tag{85}$$

simultaneously. Eliminating β_1, we find

$$84\alpha_1^2 + 36\alpha_1\epsilon + \epsilon^2 = 0, \tag{86}$$

that has no real positive solution for α_1. Thus, $\alpha_1 = 0$ is the only possible physically acceptable fixed point. RG trajectories for all initial values for α_1 and for $\beta_1 < \epsilon/2$ flow to the stable fixed point (0, 0), where as RG trajectories for all initial values for α_1 together with all initial $\beta_1 > \epsilon/2$ flow away from the origin, until they are out of the validity of our perturbation theory. This signifies instability arising from break down of linear elasticity (see below). Further, $\beta_1 = \epsilon/2 \equiv \beta_c$ is the separatrix between the stable and unstable phases. The RG flow diagram is shown in Fig. 10.

In the stable region of the phase space, linearizing about the stable fixed point (0,0), we get

$$\frac{d\alpha_1}{dl} = -\epsilon\alpha_1, \tag{87}$$

$$\frac{d\beta_1}{dl} = -\epsilon\beta_1. \tag{88}$$

These give

$$\alpha_1(l) \sim \exp(-\epsilon l),\ \ \beta_1(l) \sim \exp(-\epsilon l). \tag{89}$$

Thus, $\alpha_1(l)$ and $\beta_1(l)$ vanish exponentially in l. This gives for $\mu(l)$

$$\frac{d\mu}{dl} = g_1 - \frac{\bar{g}_1^2}{2\mu} = \mu\left[\alpha_1 - \frac{\beta_1}{2}\right]. \tag{90}$$

Thus,

$$\frac{d\mu}{dl} \to 0, \tag{91}$$

as $l \to \infty$, implying $\mu(l \to \infty) \to \mu_\infty$, a constant. Similar argument gives $\tilde{\lambda}(l \to \infty) \to \tilde{\lambda}_\infty$, another constant. Thus, there are *no infinite renormalizations* of $\mu(l)$ and $\tilde{\lambda}(l)$, unlike their 2D counterparts. Hence, there is *no* anomalous elasticity. This further means that in the thermodynamic limit, the elastic deformation fluctuations are statistically identical to that in the noninteracting theory. This immediately gives $\langle[\mathbf{u}^T(\mathbf{x})]^2\rangle$ as finite in the thermodynamic limit. This naturally corresponds to long-range order.

The separatrix is linearly unstable along the β_1 direction. This can be seen easily linearizing Eq. (39) by writing $\beta_1(l) = \beta_{1c} + \delta_2(l)$, where $\beta_{1c} = \epsilon/2$. To the linear order in δ_2, we find

$$\frac{d\delta_2}{dl} = 4\beta_c\delta_2 > 0, \tag{92}$$

clearly showing instability along both the directions parallel to the β_1 axis. However, the flow along the separatrix is *toward* the critical point $(0,\ \beta_{1c})$:

$$\left.\frac{d\alpha_1(l)}{dl}\right|_{\beta_1(l)=\beta_{1c}} = -\epsilon\alpha_1 + \frac{\alpha_1\beta_1}{2} - 3\alpha_1^2 - \frac{\beta_1^2}{8} < 0, \tag{93}$$

indicating a flow toward to the β_1 axis.

The linear instability of the fixed point $(0,\ \epsilon/2)$ together with the RG flow diagram in Fig. 10 implies that on the unstable side of the separatrix, $\beta_1(l)$ diverges for any L, so long as the initial values of α_1, β_1 lie in the unstable side of the separatrix $\beta_1 = \epsilon/2$. This further gives that for all such initial conditions renormalized μ vanishes independent of L.

Having known the structure of the RG flow lines near the fixed points for small values of the coupling constants, we can now use a Occam's razor-type argument to speculate on the global RG flow lines for arbitrary coupling constants. It is generally expected, as in 2D, that for large enough α_1 (with $\beta_1 = 0$), which may be achieved at high enough T_c, an elastic medium should melt into a liquidlike phase with SRO. It is also known that the melting transitions of crystals in 3D is indeed *first order*. Nonetheless, as argued above for 2D, the topology of the global RG flow lines should be such that the separatrix should terminate on the α_1 axis demarcating the phase with long-range positional order and the high temperature liquid phase.

We can now infer the fluctuation properties of $\mathbf{u}^L(\mathbf{x})$ directly from those of $\mathbf{u}^T(\mathbf{x})$. Here, $\beta_2 = \beta_{2c} \equiv \epsilon/8$ is separatrix, that separates the stable phase with positional order for $\beta_2(l) < \beta_{2c}$ and an unstable phase without any positional order for $\beta_2(l = 0) > \beta_{2c}$. The separatrix is linearly unstable along the β_2 direction. Again the flow along the separatrix is toward the critical point $(0,\ \beta_{2c})$. The schematic RG flow diagram in the α_2-β_2 plane is identical to Fig. 10. Again, we can construct an Occam's razor argument global RG flow lines; the corresponding flow diagram looks schematically identical to Fig. 11.

Notice that since both $\mu(l)$ and $\tilde{\lambda}(l)$ rapidly vanish (essentially as soon as the system size grows beyond a small microscopic size) on the unstable side of the separatrix, the instability is practically independent of the system size. This is in contrast to the situation at 2D. Readers interested in a perturbation theory argument for this should find one in Appendix E.

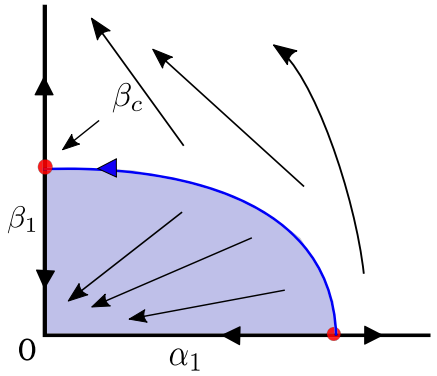

FIG. 11. Conjectured "Occam's razor" global RG flows in the α_1-β_1 plane at $d > 2$. Arrows indicate the flow directions. The light blue shaded region is the stable region. The small red circle on the α_1 axis is the putative unstable critical point not accessible in our perturbative RG. The small red circle on the β_1 axis is the unstable fixed point (see text).

VI. FIRST-ORDER TRANSITIONS

We have argued above that the nonlinear couplings of ϕ with $\mathbf{u}^T$ or $\mathbf{u}^L$ are irrelevant (in a RG sense) near the Heisenberg fixed point of the Ising model. This means the coupling with the elastic medium does not affect the second-order phase transition of the Ising model and the corresponding universal critical scaling near T_c. This however implies that the fluctuation corrected coupling constant v in Eq. (16) is *always* positive at any length scale. Can effective v be turned negative at any finite scale by large enough fluctuations? We carefully consider this question in this section.

We first consider the case with microscopic Ising symmetry, i.e., the inversion symmetry breaking couplings $\bar{g}_1$, $\bar{g}_2$ vanish. In this case, in order to have a second order transition, it should be ensured that under mode elimination, v_e, the fluctuation-corrected v at any intermediate scale never turns negative. This need not be the case always. In fact, this may not hold true for sufficiently strong order parameter-strain couplings. In the anticipation that v_e can actually turn negative, we extend $\mathcal{F}$ by adding a $v_6\phi^6$-term in it with $v_6 > 0$ for thermodynamic stability reasons. We consider the inhomogeneous fluctuation corrections to v that originate from $g_1, \bar{g}_1, g_2, \bar{g}_2$, that themselves do not depend upon v explicitly. These contributions are *finite*, but *negative*: Neglecting the homogeneous corrections to v for simplicity, and using the expressions of the diagrams in Appendix F, (with $\bar{g}_1 = 0 = \bar{g}_2$ for the microscopic inversion symmetric case) we get

$$\beta_c v_e \equiv \beta_c v - 2dT_c^2\left(\frac{\beta_c^2 g_1^2}{4\mu^2} + \frac{\beta_c^2 g_2^2}{\tilde{\lambda}^2}\right)\frac{\Lambda^d}{(2\pi)^d},$$

valid for all $d \geqslant 2$. Now, for $v_e > 0$, the $v_6\phi^6$-term is unnecessary. The phase transition of ϕ is then unaffected by the order parameter-strain couplings, and remains a continuous transition belonging to the Ising universality class. If, how-

ever, $v_e < 0$, then a $v_6\phi^6$-term must be taken into account for reasons of thermodynamic stability. In that case, ϕ now undergoes a first order transition with the order parameter $m \equiv \langle\phi\rangle$ jumping of magnitude $[|v_e|(2v_6)]^{1/2}$. We thus conclude that in ZTE systems with microscopic Ising symmetry, sufficiently strong spin-lattice couplings necessarily turn the second order transition into a first order one.

The general case with nonzero $\bar{g}_1$, $\bar{g}_2$ requires more careful scrutiny. To proceed further systematically, we generalize the free-energy functional $\mathcal{F}_\phi$ to $\tilde{\mathcal{F}}_\phi$ in general d-dimensions given by

$$\tilde{\mathcal{F}}_\phi = \mathcal{F}_\phi + \int d^dx[g\phi^3 - h\phi], \tag{94}$$

as appropriate for an *asymmetric* binary system (i.e., without any symmetry under the inversion of ϕ); parameters g and h can be of any sign. For a symmetric system $g = 0 = h$, which corresponds to an Ising magnet with no net magnetization. For a conserved system (relevant in soft matter version of this model) $\int d^dx\phi(\mathbf{x})$ is a conserved quantity (a constant), and hence drops out from (94). Clearly, free energy $\tilde{\mathcal{F}}_\phi$ in Eq. (94) in the limit of a rigid lattice (all strains vanish) generically describes a first-order transition akin to the standard liquid-gas transition. This naturally implies the existence of a coexistence curve identical to that for the liquid-gas transition, with an associated finite jump in the order parameter [6]. Nonetheless, it still admits a second-order transition at a critical point belonging to the Ising universality class. This can be shown by expanding $\tilde{\mathcal{F}}_\phi$ about $\phi = \phi_0$, with ϕ_0 is chosen in a way such that the $g\phi^3$ -term in $\tilde{\mathcal{F}}_\phi$ above vanishes. The resulting transformed free energy has the form same as that of the Ising model at a finite external magnetic field h_0 [related to h in Eq. (94) above and depends in general upon the model parameters] that has generic first-order transitions (or no transitions at all) if h_0 is tuned at any general T [6]; furthermore, second-order transitions belonging to the Ising universality class is found only if both T and h_0 are simultaneously tuned; the corresponding critical point is found in the T-h_0 plane at $r = 0$ or $T = T_c$ (in a mean-field description) and $h_0 = 0$ [6]. The coexistence curve for $\tilde{\mathcal{F}}$ above in fact is similar to that for the Ising model, except that it is now asymmetric with respect to the order parameter $\langle\phi\rangle$, averaged over the whole system due to the lack of any symmetry of $\mathcal{F}_\phi$ under inversion of ϕ. The order parameter–strain coupling terms do not change this general picture as we now discuss below.

To see the effects of the order parameter–strain couplings, we integrate out the strains from $\tilde{\mathcal{F}}$ perturbatively, a process that produces $\tilde{F}_{\phi e}$, a "dressed" $\tilde{\mathcal{F}}_\phi$ given by

$$\tilde{F}_{\phi e} = \int d^dx\left[\frac{r}{2}\phi^2 + \frac{1}{2}(\nabla\phi)^2 + v_e\phi^4 + g_e\phi^3 + v_6\phi^6 - h_e\phi\right], \tag{95}$$

where h_e is the "effective magnetic field," and v_e and g_e are the "effective" coupling constants, produced by integrating over the strains; $v_6 > 0$ is added for thermodynamic stability (see below). Here, we have ignored any corrections to r, obtained by eliminating the strain field, as they represent just a shift in T_c, a fact that is present but of little significance to the present discussion. Again, the last term on the rhs of (95) can be dropped in a conserved system.

We focus on the fluctuation-corrections to v and g that arise solely from the order parameter–strain couplings (this suffices for our purposes here). Consider the two inhomogeneous fluctuation corrections to v that originate from g_1 and $\tilde{g}_1$; which are discussed in Appendix F (see Fig. 18). Contributions from these diagrams are *finite*. and independent of v itself, i.e., inhomogeneous in. More importantly, these contribute *negatively* to v. While in the standard wisdom of RG, these *finite* corrections do not matter and are to be neglected, there is a possibility that for sufficiently large g_1 and $\bar{g}_1$, effective v actually turns negative. This then immediately destroys the assumed second-order transition, and with it all the diverging fluctuation corrections to the model parameters, since fluctuations are bounded in a first-order transition. As before, neglecting the homogeneous corrections to v and using the expressions of the diagrams in Appendix F, we define an effective v, that we denote by v_e, as follows:

$$\begin{aligned} v_e \equiv v &- 2dT_c\left(\frac{g_1^2}{4\mu^2} + \frac{g_2^2}{\tilde{\lambda}^2}\right)\frac{\Lambda^d}{(2\pi)^d} \\ &- 2dT_c\left(\frac{\bar{g}_1^4}{32\mu^4} + \frac{\bar{g}_2^4}{\tilde{\lambda}^4}\right)\frac{\Lambda^d}{(2\pi)^d}. \end{aligned} \tag{96}$$

Similarly, the inhomogeneous one-loop corrections to g are given in the Feynman graphs in Appendix F (see Fig. 19). The resulting effective parameter g_e is thus given (neglecting any homogeneous correction) by

$$\begin{aligned} g_e = g &+ g_1\bar{g}_1\frac{T_c}{2\mu^2}d\frac{\Lambda^d}{(2\pi)^d} + 2g_2\bar{g}_2\frac{T_c}{\tilde{\lambda}^2}d\frac{\Lambda^d}{(2\pi)^d} \\ &- \bar{g}_1^3\frac{T_c}{2\mu^3}d\frac{\Lambda^d}{(2\pi)^d} - 4\bar{g}_2^3\frac{T_c}{\tilde{\lambda}^3}\frac{\Lambda^d}{(2\pi)^d}. \end{aligned} \tag{97}$$

Two distinct situations can arise. First consider $g_e \neq 0$ which is the more general case. In this case, there is a generic first order transition, akin to the liquid-gas first order transition with an order parameter jump $m = -g_e/(12v)$ at a transition temperature $T^* = T_c + 9g_e^2/(16v)$ [6]. On the other hand, g_e can be turned zero by tuning g_1, $\bar{g}_1$, g_2, $\bar{g}_2$. Consider $v_e > 0$. The $v_6\phi^6$-term in Eq. (95) can now be ignored. Then Eq. (95) has the same structure as $\tilde{\mathcal{F}}_\phi$ in Eq. (94) above; the discussion that follows immediately after Eq. (94) applies here as well. By making a suitable shift in ϕ, the cubic term $g_e\phi^3$ may be eliminated from $\mathcal{F}_{\phi e}$, yielding F_e, a modified form for $\mathcal{F}_{\phi e}$, identical to the free energy for the Ising model in the presence of an external magnetic field h_ϕ. Then, the order parameter ϕ clearly generally undergoes a first-order transition below a transition temperature. A critical point with a second-order transition may still be accessed only by suitable tuning of both T and h_ϕ; in fact, the critical point is located in the T-h_ϕ plane at $r = 0$ or $T = T_c$ and $h_\phi = 0$, with an associated universal scaling behavior belonging to the 2D Ising universality class. Since h_ϕ in general depends on the order parameter–strain couplings, it is possible to tune it to zero by tuning g_1, $\bar{g}_1$, g_2, $\bar{g}_2$. Further, T_c also receives fluctuation corrections that depends on the strain–order parameter couplings (not shown here). Thus, the critical point is accessed by tuning g_1, $\bar{g}_1$, g_2, $\bar{g}_2$. At the simplest level, the role of $g_e \neq 0$ is only

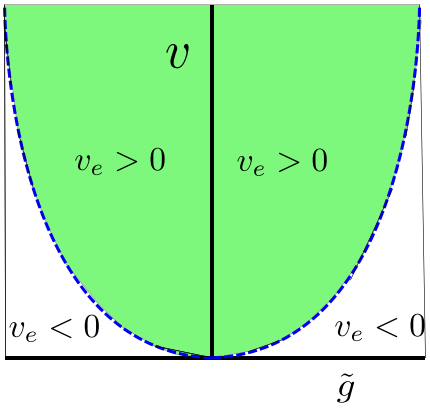

FIG. 12. Schematic phase diagram of the order parameter in the $\tilde{g} - v$ plane, where for simplicity we have set $g_1 = g_2 = \bar{g}_1 = \bar{g}_2 = \tilde{g}$. We have assumed $g_e = 0$, which rules out a first order transition of the liquid gas kind. Second order phase transition is obtained in the green region with $v_e > 0$, whereas the transition is first order in the outside white region with $v_e < 0$. The broken blue curved line is given by [see Eq. (97)] $v_e = 0$ (along with $g_e = 0$), corresponding to a line of tricritical points.

to introduce an asymmetry of the order parameter $\langle\phi\rangle$, which is reflected in the curvature of the coexistence curve at the criticality [6]. Since g_e can also be varied continuously and made positive, negative or zero by tuning the order parameter–strain coupling constants, the curvature at criticality and hence the location of the coexistence curve in the $\langle\phi\rangle$-T plane should change continuously with these coupling constants. Experimental measurements of the coexistence curve for a given system can thus reveal valuable quantitative information about these coupling constants.

If $v_e < 0$, then conditions of thermodynamic stability dictates that the $v_6\phi^6$-term in Eq. (16) must be taken into consideration, where v_6 is positive definite. We can still set g_e to zero by tuning g (in a technical language this is akin to adding a "counter term" in $\mathcal{F}$ to as to keep the net coefficient of a ϕ^3-term to zero). Now with $v_e < 0$, instead of a second-order transition, this now allows a *first-order transition* with an order parameter jump $\phi_c = \pm[|v_e|(2v_6)]^{1/2}$ at the transition temperature $T^* = T_c + 2|v_e|^2/(3v_6)$ [6]. In fact, there now exists a *tricritical point* that is determined by the condition $v_e = 0$ (along with $g_e = 0$). Notice that the dependence of v_e on the selectivity parameters $\bar{g}_1$ or $\bar{g}_2$ by a factor of 2 changes their contributions to v_e by a factor of 16, whereas similar changes in g_1, g_2 change their contributions to v_e by just a factor of 4. Thus, carefully prepared samples with different selectivity parameters should enable one to test the possibilities of both first and second-order transitions. See Fig. 12 for a schematic phase diagram.

We thus conclude that even in the presence of Ising-symmetry breaking spin-lattice coupling terms, the transition is generically first order. Nonetheless, a second order Ising transition can be accessed by tuning the model parameters reminiscent of the second order transition in liquid-gas systems. Intriguingly, this second order transition can get converted into a *different* first order one for sufficiently strong spin-lattice interactions. Across these first order transitions, the elastic modulii are finite, but still anomalous in the sense discussed below.

If there is a first-order transition, then there are no instabilities since all corrections to $\tilde{\lambda}$ and μ are finite. Nonetheless, there are corrections which can be measured. The fluctuation corrections are finite and small for small (bare) anharmonic coupling constants g_1, g_2, $\bar{g}_1$, $\bar{g}_2$. With this and neglecting the contributions from the one-loop corrections, effective μ and effective $\tilde{\lambda}$ are given by [see free-energy Eq. (16)]

$$\mu_e = \mu + g_1\langle\phi^2(\mathbf{x})\rangle + \bar{g}_1\langle\phi(\mathbf{x})\rangle, \tag{98}$$

$$\tilde{\lambda}_e = \tilde{\lambda} + 2g_2\langle\phi^2(\mathbf{x})\rangle + \bar{g}_2\langle\phi(\mathbf{x})\rangle \tag{99}$$

to the lowest order in g_1, g_2, $\bar{g}_1$, $\bar{g}_2$. For $T > T^*$, $\langle\phi^2(\mathbf{x})\rangle$ is negligible, where for $T < T^*$, $\langle\phi^2(\mathbf{x})\rangle$ can be approximated by m^2; where $m = \langle\phi(\mathbf{x})\rangle \neq 0$ is the mean field value of the order parameter below T^*. For simplicity, we neglect the one-loop corrections to g_1, g_2, $\bar{g}_1$ and $\bar{g}_2$ in this discussion. Thus,

$$\begin{aligned}\mu(T < T^*) &= \mu(T > T^*) + g_1 m^2 + \bar{g}_1 m \\ &\neq \mu(T > T^*),\end{aligned} \tag{100}$$

$$\begin{aligned}\tilde{\lambda}(T < T^*) &= \tilde{\lambda}(T > T^*) + 2g_2 m^2 + 2\bar{g}_2 m \\ &\neq \tilde{\lambda}(T > T^*).\end{aligned} \tag{101}$$

Whether or not $\mu(T < T^*)$ or $\tilde{\lambda}(T < T^*)$ is larger or smaller than their counterparts at $T > T^*$ depends on the relative values of g_1 and $\bar{g}_1$, or g_2 and $\bar{g}_2$, which are free parameters in our theory, but are actually controlled by the microscopic material properties, and the signs of $\bar{g}_1$, $\bar{g}_2$ and m. In fact, it is entirely possible that one among $\mu(T < T^*)$ and $\tilde{\lambda}(T < T^*)$ larger than its counterpart at $T > T^*$, whereas the other is smaller, since all of g_1, $\bar{g}_1$, g_2, $\bar{g}_2$ can in principle vary freely. Therefore, measurements of the elastic fluctuations should show a sudden jump across T^* and should give valuable information about the material properties. As before, for nearly incompressible systems $\tilde{\lambda}$ diverges, and we need to be concerned only with the variation of μ across the first-order transition. It is in fact possible to have instability in the ordered phase of the order parameter, leading to loss of positional order. That is any one among $\mu(T < T^*)$ and $\tilde{\lambda}(T < T^*)$ or both may be *negative*, if $\bar{g}_1$ and/or $\bar{g}_2$ are sufficiently large. Notice that this instability is independent of the system size at any dimension. A schematic phase diagram in the $\bar{g}_2^2$-μ plane may be drawn, which is topologically identical to the phase diagram valid for $T \approx T_c$, valid when there is a second-order transition; see the phase diagram in Fig. 2. In the case of first-order transition the instability exists in the entire ordered phase $T < T^*$, whereas for the second-order transition case, it is confined to the neighborhood of T_c only. More intriguingly, if the order parameter m is conserved, then below T^*, there will be (at least) two macroscopically large domains corresponding to $+m$ and $-m$. This means there is a possibility that the system remains stable in one domain, but gets unstable in the other. At the very least, the effective Lamé coefficients will be different in the different domains.

VII. CORRESPONDENCE BETWEEN THE ORDER OF THE TRANSITION AND DISPLACEMENT FLUCTUATIONS

We now elucidate the correspondence between the displacement fluctuations and the order of the associated transitions, as one crosses the transition temperature. We make the following general conclusions about the interrelations between the variances and correlations of the displacement fluctuations.

(1) At 2D

(a) If there is a second-order phase transition (i.e., with no jump in the order parameter across the transition) with the unrenormalized model parameters falling in the stable region of the phase space, then the Lamé coefficients increase as the transition temperature T_c is approached from the above. The Lamé coefficients decrease as T is further reduced below T_c. If the system size diverges, then the Lamé coefficients too diverge as T_c is approached. The system shows novel *anomalous elasticity* resulting into positional SQLRO in the thermodynamic limit, different from the well-known QLRO at $T \neq T_c$, or in a single-component elastic medium. The displacement correlation function for a large separation is much smaller than what it is away from T_c, or in a single-component medium.

(b) However, if there is a second-order phase transition and the unrenormalized model parameters fall in the unstable region of the phase space, then for a system with a finite size $L < L_c$, a critical size, the Lamé coefficients decrease as temperature T as the transition temperature T_c is approached from the above. The Lamé coefficients increase as T is further reduced below T_c. Close to T_c, the Lamé coefficients vanish as the system size L approaches L_c from below; in fact, for $L > L_c$, the system gets unstable with the attendant loss of any positional order.

(c) If there is a first-order transition at the transition temperature T^* with a finite jump in the order parameter, then there is a finite jump in the Lamé coefficients directly related to the jump in the order parameter. The displacement correlator shows conventional QLRO, with its amplitude showing a jump across the transition temperature.

(d) Independent of the order of the phase transition, the values of the Lamé coefficients above the transition temperature can be lower or higher than the corresponding values below the transition. This is controlled by the model parameters.

(2) At higher dimensions $d > 2$

(a) If there is a second-order phase transition with the unrenormalized model parameters falling in the stable region of the phase space, then the Lamé coefficients do not diverge as the critical point is approached. The system shows conventional LRO. When the unrenormalized model parameters fall in the unstable region of the phase space for any value of the system size L. This corresponds to positional short-range order only.

(b) If there is a first-order transition, then the Lamè coefficients show a jump across the transition temperature, concomitant with a jump in the displacement correlation function that shows conventional LRO below and above the transition temperature.

The above correspondences are pictorially shown in the schematic diagrams in Figs. 13 and 14.

VIII. SUMMARY

We have here developed a continuum theory of Ising transitions in a deformable isotropic zero thermal expansion elastic medium, e.g., a gel, and investigate the existence of anomalous elasticity. We consider an Ising-type scalar order parameter to describe the phase transition. Our theory includes anharmonic couplings between local in-plane lattice dilations or strains with the order parameter, such that $dT_c/dV = 0$, or $\langle u_{ij} \rangle = 0$. Further, these couplings contain two distinct anhamornic contributions, one of which respects the Ising symmetry of the order parameter in a rigid lattice, the other explicitly breaking it. The latter effectively implies selective coupling of the local strain with the local states of the order parameter, and makes the system inversion (i.e., $\mathcal{Z}_2$) asymmetric. The breaking of the $\mathcal{Z}_2$ symmetry in the present study is entirely due to its coupling with the local strain, and hence vanishes in the rigid limit of the model. These anhamornic terms are irrelevant in the RG sense when $dT_c/dV \neq 0$, and were not considered in Ref. [13]. In contrast to the present study, the absence of these anhamornic terms even at at $dT_c/dV = 0$ led Ref. [13] to conclude that spin and lattice degrees of freedom decouple in this limit.

We study the system both at 2D and $d > 2$ close to the phase transition temperature of the order parameter. At 2D, we find anomalous elasticity: When there is a second-order transition with the selectivity couplings being sufficiently weak, the in-plane displacement fluctuations are significantly suppressed in comparison with its behavior away from the phase transition; the phase transition itself remains second order belonging to the 2D Ising universality class. The elasticity is anomalous and the mean-square in-plane displacement scales as $[\ln (L/a_0)]^{2/3}$, a significantly weaker dependence on the system size L than the traditional $\ln(L/a_0)$ behavior observed in a 2D elastic medium. Similarly, the two-point correlation function of the differences in the local displacements at two points separated by a distance r scales as $[\ln(r/a_0)]^{2/3}$ for large r, a much weaker r-dependence than the well-known $\ln r$ dependence observed in QLRO. Thus, our result can be thought as a novel positional SQLRO that forms a new universality class. As the selectivity parameters grow in magnitude, the system gets unstable beyond a threshold value of the parameters as the renormalized elastic modulii vanish when the system size L exceeds a finite value. This implies a positional short-range order or SRO, reminiscent of a liquid. Thus, the selectivity parameters can introduce a novel SQLRO to SRO transition. These results are summarized in Fig. 8. Melting of 2D crystals are believed to be defect-mediated. It would be interesting to study how melting proceeds near the critical point, when the positional order is not QLRO, but SQLRO. Sufficiently strong strain-order parameter couplings can turn the phase transition to a first-order one. In that case, there is no SQLRO; conventional QLRO is observed at all temperatures. However, there are jumps in the elastic modulii as the system passes through the transition temperature. For

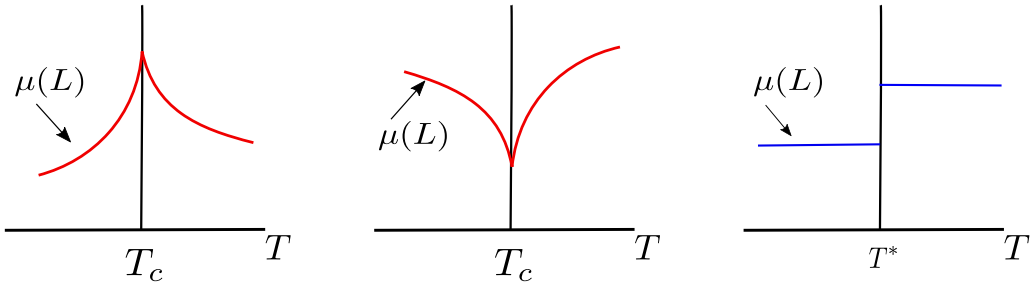

FIG. 13. Schematic variation of μ in a 2D system of finite size L across (a) a second-order transition at T_c when the unrenormalized parameters fall on the stable side of the separatrix, (b) a second-order transition at T_c when the unrenormalized parameters fall on the unstable side of the separatrix and $L < L_c$, the instability threshold, (c) a first-order transition at $T^* > T_c$, with μ having no significant L-dependence. At 3D, (c) holds regardless of the order of transitions. In all these cases, $\mu(L)$ is *smaller* in the ordered low-T phase than its value in the disordered high T-phase, which is controlled by the bare (unrenormalized) model parameters. Note the smooth variations (shown schematically) of the Lamé coefficients across second-order transitions, as opposed to their discontinuity across first-order transitions.

sufficiently strong selectivity parameters, the system can get destabilized as well.

At dimensions $d > 2$, for sufficiently weak selectivity couplings, the variance of the local elastic displacements is independent of the size of the system, corresponding to positional long-range order (LRO), not different from an ordinary 3D elastic medium, e.g., a 3D crystal. However, as the selectivity increases, the system gets unstable beyond a threshold value of the selectivity parameters, with only positional short-range order reminiscent of a liquid. Thus, a structural transition between LRO and SRO can be induced by turning the selectivity parameter. As in 2D, the phase transition can be turned to first order by tuning the selectivity parameters, across which the elastic modulii display finite jumps.

On the whole, thus, the selectivity parameters can be tuned to distabilize the positional order and also to turn the second-order phase transition to a first-order one. Assuming the selectivity parameters to be continuously varying control parameters, we can note that such variations lead to *re-entrant structural phase transitions* of the sample; this could be easily seen if one moves along the $\bar{g}_1$ axis in the phase diagram Figs. 1 and 2.

The free energy $\mathcal{F}$ in Eq. (16) for ZTE elastic media is constructed in such a way that $\langle u_{ij} \rangle = 0$ identically in the absence of externally applied stresses, ensuring vanishing thermal expansion. If we relax this condition, then additional terms of the form $\int d^d x \hat{g}_A A(\phi) u_{ii}$ can be added to $\mathcal{F}_{u\phi}$ in Eq. (8) above, where $A(\phi)$ is a generic polynomial function of ϕ, which would lead to thermal expansion $\propto g_A \langle A(\phi) \rangle$ (which vanishes automatically in the incompressible limit). Such a term with $A(\phi) = A_0\phi + A_1\phi^2 + \cdots$, being more relevant than the existing order parameter–elastic deformation anhamornic terms, can distablize the RG fixed points discussed here; see also Ref. [13]. These terms would then describe materials with finite thermal expansions. However, in nearly compressible systems, u_{ii} is small, and there should be a sufficiently large scales over which the physics described here could be observed.

The stiffening of the system with weak selectivity at 2D holds close to the critical point only. Away from the critical point, all the fluctuation corrections are finite. These finite

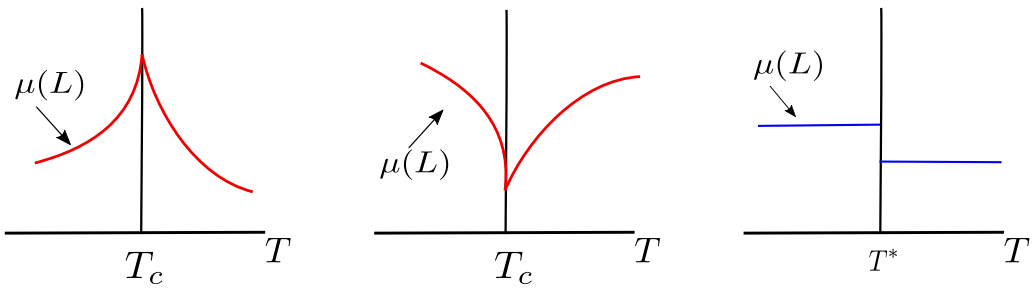

FIG. 14. Schematic variation of μ in a 2D system of finite size L across (a) a second-order transition at T_c, when the unrenormalized parameters fall on the stable side of the separatrix, (b) a second-order transition at T_c when the unrenormalized parameters fall on the unstable side of the separatrix and $L < L_c$, the instability threshold, (c) a first-order transition at $T^* > T_c$, with μ having no significant L-dependence. At 3D, (c) holds regardless of the order of transitions. In all these cases, $\mu(L)$ is *larger* in the ordered low-T phase than its value in the disordered high T-phase, which is controlled by the bare (unrenormalized) model parameters. Note the smooth variations (shown schematically) of the Lamé coefficients across second-order transitions, as opposed to their discontinuity across first-order transitions.

corrections to μ and $\tilde{\lambda}$ can however turn these elastic modulii negative, if the selectivity parameters are large enough. However, these instabilities no longer depend upon the system size. For weak selectivity, μ and $\tilde{\lambda}$ remain positive, but finite, leading to the standard QLRO. Thus, phase diagrams in Figs. 1 and 2 still hold with the caveat that the positional order now refers to just QLRO. This picture holds in 3D as well.

In general, thermal expansion could be controlled or significantly restricted by various means, e.g., by inclusion of additives or impurities with negative thermal expansion coefficient [34], such that results predicted by theory could be observed over a large range of length scales. Our theory is generic, and applicable to Ising transitions in any isotropic elastic medium, independent of its microscopic details. This theory can be tested in numerical simulations of appropriately constructed spin-lattice models near phase transitions in models with ZTE or the condition $dT_c/dV = 0$, and also by performing controlled experiment on ZTE materials having phase transitions within the temperature range of ZTE behavior. Recent progress in the synthesis of two-component ZTE materials [35] are promising developments in this direction. We expect future technological breakthrough will make it possible to design specific ZTE materials where our theory can be tested. Possible stiffening of ZTE materials near second-order transitions may make such materials highly valuable in making precision engineering equipment. We look forward to future research in these directions.

Our work can be extended in several ways. First, we have assumed an isotropic elastic medium. It would be interesting to study how anisotropy would affect our results. Then, to keep the theory simple, we have just considered a continuous medium coupled with Ising spins. More realistic situations, in particular, biologically relevant ones, may involve several lipids, requiring multiple order parameters. This can potentially give rise to multicritical points, or even simultaneous occurrence of first and second-order transitions. The nature of any anomalous elasticity, and the displacement fluctuations in such systems remain open questions. It will be interesting to study the dynamics of the fluctuations and the spatiotemporal scaling of the time-dependent correlation functions of the displacements near the second-order transitions. Furthermore, extending these ideas to "active" or nonequilibrium systems should be important, with possible strong relevance to biological systems, e.g., phase separations in biological cells, or flocking phenomena in a correlated background due to a second-order phase transition. Further work should be undertaken in this context.

ACKNOWLEDGMENTS

We thank T. Das for comments and suggestions. S.M. thanks the SERB, DST (India) for partial financial support through the TARE scheme (Grant No. TAR/2021/000170). A.B. thanks the SERB, DST (India) for partial financial support through the MATRICS scheme (Grant No. MTR/2020/000406).

APPENDIX A: GLOSSARY

In this Appendix, we list and give rough definitions for the symbols used in this paper, in the order in which they appear in the text. We also refer to the equations that precisely define them, or where they appear first in the text.

(1) $\tilde{\mathcal{F}}$: Total free energy of the system [Eq. (5)].

(2) $\mathcal{F}_\phi$: Free energy for the Ising degrees of freedom [Eq. (6)].

(3) $r = T - T_c$: Difference between the temperature T (not to be confused with superscript T in $\mathbf{u}^T$) and the mean-field critical temperature T_c of the Ising degrees of freedom [Eq. (6)].

(4) $v > 0$: Anharmonic coupling constant that couples ϕ's with itself [Eq. (6)].

(5) $\mathcal{F}_u$: Free energy for the local displacements u_i [Eq. (7)].

(6) μ, λ: Bare Lamé coefficients for the in-plane elasticity of the system [Eq. (7)].

(7) $u_{ij} = \frac{1}{2}(\nabla_i u_j + \nabla_j u_i)$ is the local strain [Eq. (7)].

(8) $\mathcal{F}_{u\phi}$: Free energy of interactions between the order parameter ϕ and displacement u_i [Eq. (8)].

(9) $\bar{g}_{10}$, $\bar{g}_2$: Anhamornic coupling constants which couple order parameter linearly with the local displacement and *explicitly break* the inversion symmetry of ϕ in $\mathcal{F}_\phi$ [Eq. (8)].

(10) g_{10}, g_2: Anhamornic coupling constants which couple order parameter quadratically with the local displacements, and *maintain* the inversion symmetry of ϕ in $\mathcal{F}_\phi$ [Eq. (8)].

(11) $\mathbf{u}^L(\mathbf{q})$, $\mathbf{u}^T(\mathbf{q})$: Longitudinal and transverse components of the displacement $\mathbf{u}(\mathbf{q})$, written in the Fourier space [Eq. (14)].

(12) L: Linear system size (not to be confused with superscript L in $\mathbf{u}^L$).

(13) a_0: Short distance cutoff [Eq. (21)].

(14) $\Lambda = 2\pi/a_0$: Upper wave-vector cutoff [Eq. (25)].

(15) $\tilde{\lambda} = \lambda + 2\mu$: Effective elastic modulus [Eq. (16)].

(16) C_v: Specific heat at constant volume [Eq. (27)].

(17) $\epsilon = d - 2$: Small parameter in the RG calculation [Eq. (32)].

(18) $\alpha_1 = \frac{T_c g_1 S_d}{(2\pi)^d \mu}\Lambda^\epsilon$, $\beta_1 = \frac{T_c \bar{g}_1^2 S_d}{(2\pi)^d \mu^2}\Lambda^\epsilon$: Effective coupling constants [Eq. (36)].

(19) $\alpha_2 = \frac{T_c g_2 S_d}{(2\pi)^d \tilde{\lambda}}\Lambda^\epsilon$, $\beta_2 = \frac{T_c \bar{g}_2^2 S_d}{(2\pi)^d \tilde{\lambda}^2}\Lambda^\epsilon$: Effective coupling constants [Eq. (37)].

(20) Γ_{1c}: Slope of the separatrix in the α_1-β_1 plane in 2D [Eq. (45)].

(21) δ_1: (Small) deviation from the separatrix in the α_1-β_1 plane in 2D [Eq. (48)].

(22) $\tilde{\lambda}(q)$: Renormalized wave-vector-dependent elastic modulus [Eq. (56)].

(23) ξ_{NL}: Length scale at which the anharmonic effects become important [Eq. (58)].

(24) L_c: Position correlation length, or the length at which $\mu(L_c) \approx 0$ [Eq. (72)].

(25) Γ_{2c}: Slope of the separatrix in the α_2-β_2 plane in 2D [Eq. (79)].

(26) δ_2: (Small) deviation from the separatrix in the α_2-β_2 plane in 3D [Eq. (92)].

(27) $\tilde{\mathcal{F}}_\phi$: Free energy of the Ising degrees of freedom that includes a ϕ^3 and linear ϕ terms [Eq. (94)].

(28) g: Coefficient of the ϕ^3 term in $\tilde{\mathcal{F}}_\phi$ [Eq. (94)].

(29) h: Thermodynamic conjugate to ϕ—"magnetic field"; coefficient of the linear ϕ-term in $\tilde{\mathcal{F}}_\phi$ [Eq. (94)].

APPENDIX B: PARAMETER ESTIMATES

We begin by noting that both the elastic modulii have the dimensions of energy/length^d $\sim k_BT$/length^d in d dimensions. Taking this length to be the small scale $\sim a_0$, which is the mesh size of a cross linked polymer network, or the lattice spacing for a crystal, we get

$$\mu, \lambda \sim k_BT/a_0^d. \tag{B1}$$

We take $a_0 \sim 60$ nm for a spectrin network [36]. Typical shear modulus of a 2D spectrin network are $\mu \sim 10^{-5}$ J/m^2 [37]; for an incompressible medium $\tilde{\lambda} \gg \mu$.

We can now find out the dimensions of $g_{1,2}$ and $\bar{g}_{1,2}$. We start from the fact that

$$\int d^dx g_{1,2}\phi^2(\nabla_i u_j)^2 \sim k_BT \sim \int d^dx \bar{g}_{1,2}\phi(\nabla_i u_j)^2, \tag{B2}$$

giving

$$[g_{1,2}\phi^2] \sim k_BT/a_0^d \sim [\bar{g}_{1,2}\phi]; \tag{B3}$$

where [...] implies "in a dimensional sense." Now for a two-component system, if we assume ϕ to be the concentration or number density difference between the two components, then $[\phi] \sim 1/a^d$. In this case, the dimensions of $g_{1,2}$ differ from those of $\bar{g}_{1,2}$. However, if ϕ is a magnetic (Ising) spin, then ϕ may be chosen dimensionless. In this case, $g_{1,2}$ and $\bar{g}_{1,2}$ have the same dimensions.

APPENDIX C: FREE ENERGY

We first derive the free energy $\mathcal{F}$ in Eq. (16). We split

$$u_i(\mathbf{q}) = P_{ij}(\mathbf{q})u_j(\mathbf{q}) + Q_{ij}(\mathbf{q})u_j(\mathbf{q}) = u_i^T(\mathbf{q}) + u_i^L(\mathbf{q}). \tag{C1}$$

Next we note that

$$\begin{aligned}\int d^dx u_i^T(\mathbf{x})\, u_i^L(\mathbf{x}) &= \int \frac{d^dq}{(2\pi)^d} u_i(-\mathbf{q})^T\, u_i^L(\mathbf{q}) \\ &= \int \frac{d^dq}{(2\pi)^d} P_{ij}(\mathbf{q})Q_{im}(\mathbf{q})u_j^T(-\mathbf{q})u_n^T(\mathbf{q}) = 0,\end{aligned} \tag{C2}$$

where we have used $P_{ij}(\mathbf{q})Q_{ij}(\mathbf{q}) = 0$. Furthermore,

$$\begin{aligned}\int d^dx[u_{ii}(\mathbf{x})]^2 &= \int d^dx[\partial_i u_j^L(\mathbf{x})][\partial_j u_i^L(\mathbf{x})] \\ &= \int d^dx[\partial_i u_j^L(\mathbf{x})][\partial_i u_j^L(\mathbf{x})] \\ &= \int d^dx[\partial_i u_j^L(\mathbf{x})]^2.\end{aligned} \tag{C3}$$

Now use that

$$\begin{aligned}\int d^dx(\nabla_i u_j)^2 &= \int \frac{d^dq}{(2\pi)^d} q^2 \mathbf{u}(\mathbf{q})\cdot\mathbf{u}(-\mathbf{q}) \\ &= \int \frac{d^dq}{(2\pi)^d} q^2[\mathbf{u}^L(\mathbf{q})\cdot\mathbf{u}^L(-\mathbf{q}) \\ &\quad + \mathbf{u}^T(\mathbf{q})\cdot\mathbf{u}^T(-\mathbf{q})] \\ &= \int d^dx\left[\left(\nabla_i u_j^L\right)^2 + \left(\nabla_i u_j^T\right)^2\right].\end{aligned} \tag{C4}$$

Substituting this decomposition, we get Eq. (16), and also Eq. (18) at the harmonic order.

APPENDIX D: RG CALCULATION

1. Upper critical dimensions

To determine the upper critical dimensions of the various anhamornic terms, we rescale space and obtain the corresponding scaling of the model parameters. We rescale space and the fields as follows ($b > 1$):

$$\mathbf{x}' = \frac{\mathbf{x}}{b}, \tag{D1}$$

$$u_i(\mathbf{x}) = \zeta_u u(\mathbf{x}') = \zeta_u u_i(\mathbf{x}/b), \tag{D2}$$

$$\phi(\mathbf{x}) = \zeta_\phi \phi(\mathbf{x}') = \zeta_\phi \phi(\mathbf{x}/b). \tag{D3}$$

These rescaling factors may be calculated by demanding that under naïve rescaling, bare μ, $\tilde{\lambda}$ do not scale, and the coefficient of the term $\int d^dx(\nabla\phi)^2$ remains unity under rescaling. This gives

$$\zeta_u = \zeta_\phi = b^{1-d/2}. \tag{D4}$$

We can use Eq. (D4) to obtain how the anhamornic coupling constants change under naïve rescaling. We find

$$u' = b^{4-d}u, \quad g_a' = b^{2-d}g_a, \quad \bar{g}_a' = b^{2-d}\bar{g}_a, \tag{D5}$$

$a = 1, 2$. Thus, critical dimension of u is 4, and the critical dimension of g_1, g_2, $\bar{g}_1$, and $\bar{g}_2$ is 2.

2. Feynman diagrams

The one-loop integrals for μ, $\tilde{\lambda}$, g_1, $\bar{g}_1$, g_2, and $\bar{g}_2$ are all evaluated at $T = T_c$.

We first consider the one-loop Feynman graphs in Fig. 5 that renormalize μ.

Diagram 5(a) has the value

$$-g_1\int_{\Lambda/b}^{\Lambda}\frac{d^dq}{(2\pi)^d}\langle|\phi(\mathbf{q})|^2\rangle = -g_1\langle\phi^{>2}(\mathbf{x})\rangle = -g_1\frac{T_c}{2\mu}\delta l \tag{D6}$$

in all dimensions. Similarly, diagram 5(b) contributes

$$\bar{g}_1^2\frac{T_c}{2\mu}\int_{\Lambda/b}^{\Lambda}\frac{d^dq}{(2\pi)^d}\langle|\phi(\mathbf{q})|^2\rangle = \bar{g}_1^2\frac{T_c^2}{2\mu}\delta l, \tag{D7}$$

in all dimensions. Similarly, evaluating the diagrams for μ in Fig. 5, we obtain by combining both the corrections

$$\mu^< = \mu + g_1 - \frac{T_c\bar{g}_1^2}{2\mu}. \tag{D8}$$

The one-loop diagrams which correct $\tilde{\lambda}$ are given in Fig. 15.

Proceeding as before, we obtain

$$\tilde{\lambda}^< = \tilde{\lambda} + 2g_2 - \frac{2T_c\bar{g}_2^2}{\tilde{\lambda}}. \tag{D9}$$

We now consider the one-loop fluctuation corrections to g_1 and $\bar{g}_1$. We obtain

$$g_1^< = g_1 - \left(\frac{4T_cg_1^2}{d\mu^2} + \frac{\bar{g}_1^4}{4d\mu^3}\right)\langle\phi^2(\mathbf{x})^>\rangle, \tag{D10}$$

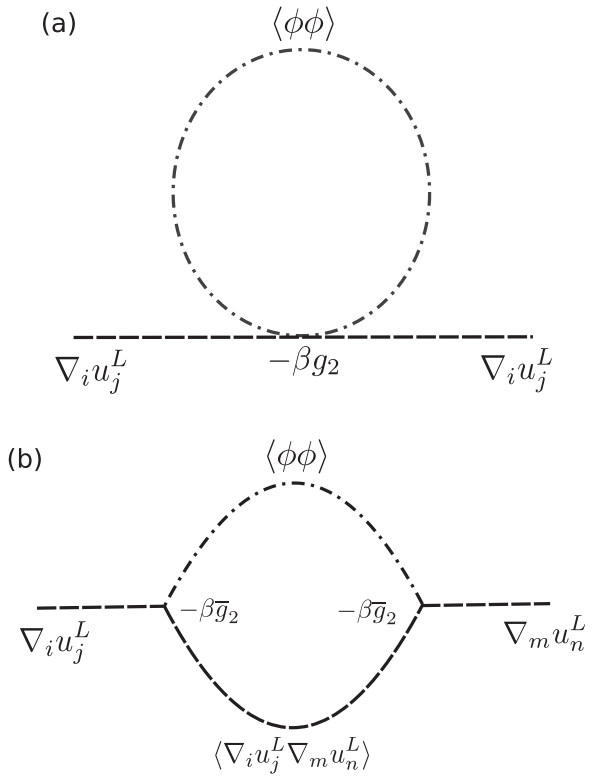

FIG. 15. One-loop diagrams that contribute to the fluctuation corrections of $\tilde{\lambda}$. Diagram (a) comes from the nonlinear coupling g_2, where as diagram (b) comes from $\overline{g}_2$ (see text).

$$\overline{g}_1^{<} = \overline{g}_1 + \left(\frac{\overline{g}_1^3}{d\mu^2} - \frac{4g_1\overline{g}_1}{\mu}\right)\langle\phi^2(\mathbf{x})^{>}\rangle. \tag{D11}$$

Using the expression for $\langle\phi^2(\mathbf{x})\rangle$, $g_1^{<}$, $\overline{g}_1^{<}$ can be calculated.

The one-loop diagrams that correct g_2 and $\overline{g}_2$ are shown in Figs. 16 and 17.

Having shown that all the one-loop corrections are proportional to $\langle\phi^{>2}(\mathbf{x})\rangle$, we are now obliged to discuss the evaluation of $\langle\phi^{>2}(\mathbf{x})\rangle$.

As we have argued above, at 2D $\langle\phi^2(\mathbf{x})\rangle \sim T_c \ln|(T - T_c)/T_c|$ as $T \to T_c$. Using $\xi \sim [(T - T_c)/T_c]^{-\nu}$, we get $\langle\phi^2(\mathbf{x})\rangle \sim T_c \ln\xi/a_0 \times \mathcal{O}(1)$. This gives

$$\langle\phi^{>2}(\mathbf{x})\rangle \sim T_c \ln b \times \mathcal{O}(1). \tag{D12}$$

Thus, the contribution from diagram 5(a) reads

$$-g_1 T_c \ln b \approx -g_1 T_c \delta l \tag{D13}$$

in 2D, where $b = \exp(\delta\ell) \approx 1 + \delta l$ for small δl. However, at $d > 2$, proceeding similarly,

$$\langle\phi^{>2}(\mathbf{x})\rangle \sim T_c \frac{\Lambda^{-\alpha+1}}{-\alpha+1}[1 - b^{-\alpha+1}] \approx T_c \delta l. \tag{D14}$$

Thus, the contribution from diagram 5(a) at $d > 2$ again reads

$$-g_1 T_c \delta l. \tag{D15}$$

In each of Eqs. (D13) and (D15), we have absorbed $\mathcal{O}(1)$ constants, that arises in the evaluation of the diagrams, into the definitions of g_1, g_2, $\overline{g}_1$, and $\overline{g}_2$ without any loss of generality.

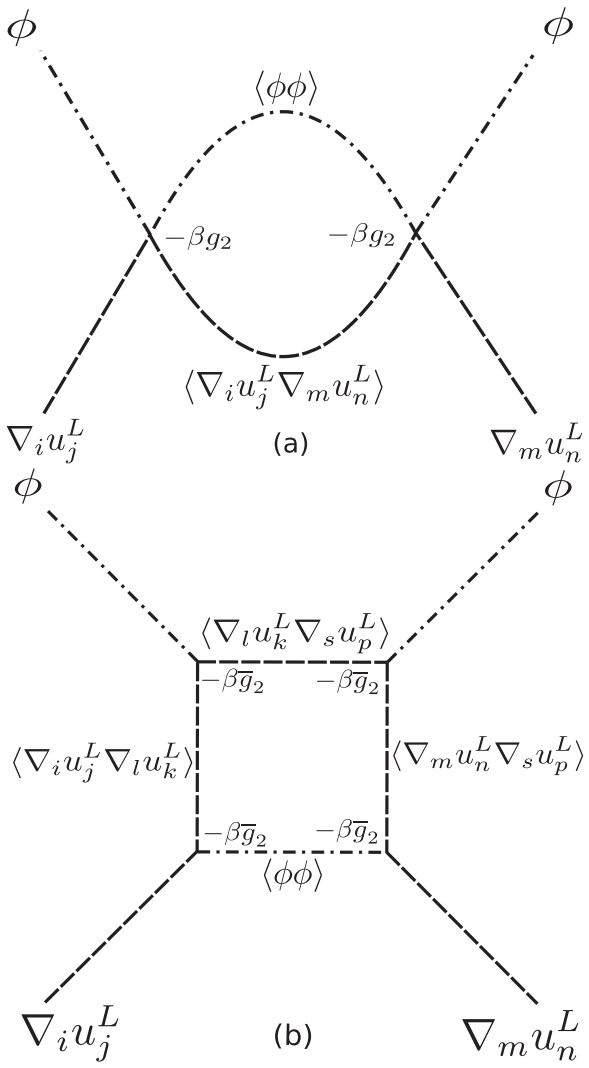

FIG. 16. One-loop diagrams that contribute to the fluctuation corrections of g_2. Diagram (a) depends only on g_2, whereas diagram (b) depends only on $\overline{g}_2$.

3. Variances $\langle(\nabla_i u_j^T)^2\rangle$ and $\langle(\nabla_i u_j^L)^2\rangle$ in 2D

We now recalculate $\langle(\nabla_i u_j^T)^2\rangle$ and $\langle(\nabla_i u_j^L)^2\rangle$ by using the forms of the renormalized propagators for $u_i^T(\mathbf{q})$ and $u_i^L(\mathbf{q})$ that is valid up to an upper wave-vector limit Λ. We note that the form of $\langle|\mathbf{u}^T(\mathbf{q})|^2\rangle$ valid up to an upper wave-vector limit Λ should read

$$\begin{aligned}\langle|\mathbf{u}^T(\mathbf{q})|^2\rangle &\approx \frac{T_c}{4\pi}[\mu_R \ln(\Lambda/q)]^{2/3} q^2]^{-1}, \quad q < 1/\xi_{NL},\\ \langle|\mathbf{u}^T(\mathbf{q})|^2\rangle &\approx \frac{T_c}{4\pi\mu q^2}, \quad 1/\xi_{NL} < q < \Lambda.\end{aligned} \tag{D16}$$

Inverse Fourier transform of Eq. (D16) gives

$$\begin{aligned}\langle[\mathbf{u}^T(\mathbf{x})]^2\rangle &= \int_{2\pi/L}^{\Lambda} \frac{d^2q}{(2\pi)^2}\langle|\mathbf{u}^T(\mathbf{q})|^2\rangle\\ &= \frac{T_c}{2\mu_R}\left[\int_{2\pi/L}^{C'} + \int_{C'}^{\Lambda}\right]\frac{d^2q}{(2\pi)^2}\langle|\mathbf{u}^T(\mathbf{q})|^2\rangle\end{aligned}$$

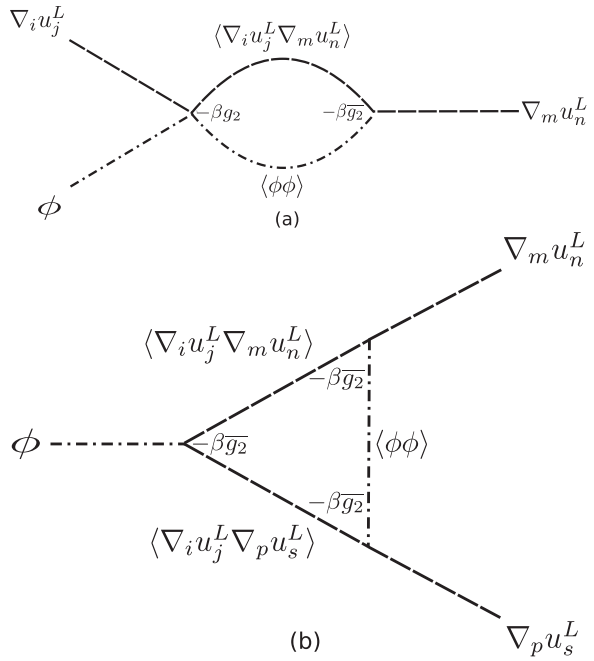

FIG. 17. One-loop diagrams that contribute to the fluctuation corrections of $\bar{g}_2$. Diagram (a) depends both g_2 and $\bar{g}_2$, whereas diagram (b) depends only on $\bar{g}_2$.

$$= \frac{T_c}{2\mu_R}\int_{2\pi/L}^{C'} \frac{d^2q}{(2\pi)^2}\frac{1}{[q^2\{\ln(\Lambda/q)\}^{1/3}]} + \int_{C'}^{\Lambda}\frac{d^2q}{(2\pi)^2}\langle|\mathbf{u}^T(\mathbf{q})|^2\rangle, \tag{D17}$$

where $C' < 1/\xi_{NL}$, $C' \sim \mathcal{O}(1)$ is such that in the range $2\pi/L < q < C'$, $\langle|\mathbf{u}^T(\mathbf{q})|^2\rangle$ is well approximated by $[T_c/(2\mu_R)]1/[q^2\{\ln|\Lambda/q|\}^{1/3}]$. This integral scales with L as $[\ln(C'L)]^{2/3}$. The remaining integral is independent of L. We thus conclude that

$$\langle[\mathbf{u}^T(\mathbf{x})]^2\rangle = \frac{T_c}{4\pi\mu_0}[\ln(C'L)]^{2/3} + \mathcal{O}(1) \approx \frac{T_c}{4\pi\mu_0}[\ln(C'L)]^{2/3}, \tag{D18}$$

for large L, same as what we have obtained above [see Eq. (59)].

4. Correlation functions in 2D

We are interested in calculating the correlation functions of $u_i(\mathbf{x})$, defined as

$$C^a_{uu}(r) \equiv \left\langle\left[u_i^a(\mathbf{x}) - u_i^a(\mathbf{x}')\right]^2\right\rangle, \tag{D19}$$

where $a = L$ or T, corresponding to u_i^L or u_i^T, in 2D near $T = T_c$; $\tilde{r} = |\mathbf{x} - \mathbf{x}'|$. We first revisit the correlator in the Fourier space in the harmonic theory, in which at T_c,

$$C^a_{uu0}(k) \equiv \left\langle u_i^a(\mathbf{k})u_i^a(-\mathbf{k})\right\rangle = \frac{T_c}{\tilde{a}k^2}, \tag{D20}$$

where $\tilde{a} = 2\mu$, $\tilde{\lambda}$ for $a = T$, L, respectively, for the transverse and longitudinal components of $\mathbf{u}(\mathbf{x})$; a subscript "0" refers to $C_{uu}(\tilde{r})$ being evaluated in the Gaussian theory, i.e., after setting all the anhamornic couplings to zero. Note that (D20) holds at all T. Inverse Fourier transform of Eq. (D20) gives the correlation function $C^a_{uu}(\tilde{r})$ in the real space in the harmonic theory:

$$\begin{aligned} C^a_{uu0}(\tilde{r}) &= 2\int_0^{\Lambda}\frac{d^2k}{(2\pi)^2}[1 - \exp i\mathbf{k}\cdot(\mathbf{x}-\mathbf{x}')]\frac{T_c}{\tilde{a}k^2} \\ &= \frac{2T_c}{(2\pi)^2}\int_0^{\Lambda}\frac{dk}{\tilde{a}k}\int_0^{2\pi}(1 - \exp[ik\tilde{r}\cos\theta]) \\ &= \frac{2T_c}{(2\pi)^2}\int_0^{1}\frac{dq}{\tilde{a}k}\int_0^{2\pi}(1 - \exp[iqy\cos\theta]) \\ &\equiv I_0(y), \end{aligned} \tag{D21}$$

where $q = k/\Lambda$ and $y = \Lambda\tilde{r}$. Then,

$$\begin{aligned} \frac{dI_0}{dy} &= \frac{-2iT_c}{\tilde{a}(2\pi)^2}\int_0^1 dq\int_0^{2\pi}\cos\theta\exp[iqy\cos\theta]\,d\theta \\ &= \frac{-2iT_c}{\tilde{a}y(2\pi)^2}\int_0^{y} du\int_0^{2\pi} d\theta\,\cos\theta\exp[iqy\cos\theta] \\ &= \frac{-2iT_c}{\tilde{a}y(2\pi)^2}\int_0^{2\pi} d\theta\,\cos\theta\int_0^{\infty} du\exp[iqy\cos\theta] \\ &= \frac{-2iT_c}{\tilde{a}y(2\pi)^2}\int_0^{2\pi} d\theta\,\cos\theta\left[\pi\delta(\cos\theta) + i\mathcal{P}\left(\frac{1}{\cos\theta}\right)\right], \end{aligned} \tag{D22}$$

in the limit $\tilde{r} \to \infty$. Now, $\delta(\cos\theta)$ is even under $\theta \to \theta + \pi$, but $\cos\theta$ is odd under the same. Hence, the contribution from the $\delta(\cos\theta)$ part of the integrand vanishes. In contrast, $\mathcal{P}(\frac{1}{\cos\theta})$ is odd, and hence the corresponding contribution survives. Therefore,

$$\begin{aligned} \frac{dI_0}{dy} &= \frac{2T_c}{\tilde{a}(2\pi)^2}\int_0^{2\pi} d\theta\,\cos\theta\,\mathcal{P}\left(\frac{1}{\cos\theta}\right) \\ &= \frac{T_c}{\tilde{a}\pi y}. \end{aligned} \tag{D23}$$

Therefore,

$$C^a_{uu0}(\tilde{r}) = \frac{T}{\pi\tilde{a}}\ln(\Lambda\,\tilde{r}), \tag{D24}$$

for $\tilde{r} \to \infty$, giving QLRO. As expected, this is valid at all temperature T.

We now calculate $C^a_{uu}(\tilde{r})$ in the anhamornic, renormalized theory at $T = T_c$. We start from

$$\left\langle u_i^a(\mathbf{k})u_i^a(-\mathbf{k})\right\rangle \approx \frac{T_c}{a_R k^2|\ln(\Lambda/k)|^{1/3}}, \tag{D25}$$

where $a_R = 2\mu_R$, $\tilde{\lambda}_R$. Equation (D25) is no longer valid over the wave-vector range from 0 to Λ, rather it is valid between 0 and $\tilde{\Lambda} \ll \Lambda$.

The renormalized correlation function in the real space is then given as

$$C^a_{uu}(r) \approx \int_0^{\Lambda}\frac{d^2k}{(2\pi)^2}[1 - \exp i\mathbf{k}\cdot(\mathbf{x}-\mathbf{x}')] \times \frac{2T_c}{a_R k^2[\ln(\Lambda/k)]^{1/3}}. \tag{D26}$$

Integrating over the angular variable, we get

$$C^a_{uu}(r) \approx \int_0^{\tilde{\Lambda}} \frac{dq\,2T_c}{a_R q|\ln(q/\Lambda)|^{1/3}}\left[\frac{1}{2\pi}\int_0^{2\pi} d\theta(1-e^{iqr\cos\theta}\right]$$
$$= \int_0^{\tilde{\Lambda}} \frac{dq\,2T_c}{a_R q|\ln(q/\Lambda)|^{1/3}}[1-J_0(qr)]$$
$$= \int_0^{\tilde{\Lambda}r} \frac{du\,2T_c[1-J_0(u)]}{a_R u|\ln(\frac{u}{x\Lambda})|^{1/3}}, \tag{D27}$$

where $J_0(u)$ is the Bessel function of order zero. Then

$$C^a_{uu}(r) = \int_0^1 \frac{du\,2T_c[1-J_0(u)]}{a_R u[\ln u+\ln(1/y)]^{1/3}}$$
$$+\int_1^{\tilde{\Lambda}r} \frac{du\,2T_c}{a_R u\{\ln u+\ln[1/(\Lambda r)]\}^{1/3}}$$
$$-\int_1^{\tilde{\Lambda}r} \frac{du\,2T_c J_0(u)}{a_R u\{\ln u+\ln[1/(\Lambda r)]\}^{1/3}}. \tag{D28}$$

Since $u_{\max}=\tilde{\Lambda}r \ll \Lambda r$, the second contribution on the right may be evaluated by setting $u=\exp(z)$. This gives

$$\int_1^{\tilde{\Lambda}r} \frac{du}{a_R u[\ln(\Lambda r)]^{1/3}} \approx \frac{2}{3}[\ln(\Lambda r)]^{2/3}+\text{const.} \tag{D29}$$

We thus find $C^a_{uu}(r)\approx \frac{T_c}{a_R}|\ln(\Lambda r)|^{2/3}$ in the limit of large r, with the remaining contributions on the right-hand side of Eq. (D28) being finite or subleading for large r. By using the above procedure, we recover the scaling of the harmonic theory or QLRO. We find that $C^a_{uu}(r)(r)$ eventually does diverge in the thermodynamic limit, but does so much slower than the corresponding result with QLRO:

$$C^a_{uu}(r)/C^a_{0uu}(r)\to 0 \tag{D30}$$

for large r. Naturally, we call this positional order stronger than QLRO (SQLRO).

APPENDIX E: POSITIONAL CORRELATION LENGTH IN THE PERTURBATION THEORY

We can obtain the positional correlation length from the fluctuation corrected μ or $\tilde{\lambda}$ from the one-loop bare perturbation theory. Let us first focus on 2D. The calculation is essentially same as the RG calculations in Appendix D above, except that we now extend the integrals over wave vectors down to an infra-red cut-off $q_{\min}\equiv 2\pi/L$, where L is the length scale at which we intend to calculate the effective values μ_e and $\tilde{\lambda}_e$, respectively, of μ and $\tilde{\lambda}$. Evaluating the leading order (i.e., one-loop) perturbative corrections to μ coming from wave vectors $q>2\pi/L$, we obtain at 2D

$$\mu_e(L)=\mu+\left(g_1-\frac{\bar{g}_1^2}{2\mu}\right)\frac{T_c}{2\pi}\ln(L/a_0), \tag{E1}$$

where as usual g_1, $\bar{g}_1$ refer to the bare or unrenormalised parameters used in the free energy $\mathcal{F}$ in Eq. (16). A similar perturbative expansion for $\tilde{\lambda}_e$ may be written. Evidently, for a sufficiently large $L=L_c$, μ_e can be made zero. We get the following relation for $\mu_e(L=L_c)=0$:

$$\mu=\left(\frac{\bar{g}_1^2}{2\mu}-g_1\right)\frac{T_c}{2\pi}\ln(L_c/a_0), \tag{E2}$$

$$L_c=a_0\exp\left[\frac{\mu}{\left(\frac{\bar{g}_1^2}{2\mu}-g_1\right)}\frac{2\pi}{T_c}\right]. \tag{E3}$$

Thus, as $g_1\to\frac{\bar{g}_1^2}{2\mu}$ from below, $L_c\to\infty$. for $L<L_c$, the system remains stable with positional order. This critical length L_c, being the linear size of the system such that $\mu_e(L_c)=0$, can be identified with a persistence length or positional correlation length ξ: As L exceeds ξ, positional correlations are lost. When L_c is plotted as a function of $\bar{g}_1^2$ for a given μ, the phase diagram in Fig. 3 in the $\bar{g}_1^2$-L plane is obtained.

We are interested in the parameter regimes where μ_e, $\tilde{\lambda}_e>0$ (our perturbation theory becomes meaningless outside this regime). Clearly, if

$$g_1-\frac{\bar{g}_1^2}{2\mu}>0, \tag{E4}$$

then we have $\mu_e>\mu$, i.e., stiffening of the shear modulus. This corresponds to the stable side of the separatrix Eq. (8) in the RG calculations. However, if

$$g_1-\frac{\bar{g}_1^2}{2\mu}<0, \tag{E5}$$

then $\mu_e<\mu$ necessarily. Thus,

$$\frac{\bar{g}_1^2}{\mu g_1}=2 \tag{E6}$$

is the borderline of stability. Note that this essentially same as Eq. (47) above; the slight difference in the right-hand side of the two is attributed to the quantitative difference between the renormalized perturbation theory and ordinary perturbation theory. Nonetheless, Eq. (E6) produces the same phase diagrams as Figs. 1 and 2.

Similar analysis for $\tilde{\lambda}_e$ yields an exactly analogous expression for a critical size for the longitudinal modes. See phase diagrams in Figs. 3 and 2.

We now consider the three-dimensional case. An equation that is a direct analog of Eq. (E1) can be written as below. We note that at 3D, the leading order corrections, i.e., the relevant integrals, can be performed all the way down to wave vector $q=0$ without encountering any divergence from the lower limits of the integrals. This yields

$$\mu_e=\mu+\left(g_1-\frac{\bar{g}_1^2}{2\mu}\right)\frac{T_c\Lambda}{2\pi}. \tag{E7}$$

Similar to the 2D case, if $g_1-\frac{\bar{g}_1^2}{2\mu}>0$, then $\mu_e>\mu$; else, $\mu_e<\mu$. In that latter case, $\mu_e=0$ sets the threshold for instability and breakdown of the positional order. We find

$$\mu=\left(\frac{\bar{g}_1^2}{2\mu_0}-g_1\right)\frac{T_c\Lambda}{2\pi}. \tag{E8}$$

Unlike its 2D counterpart, Eq. (E8) is independent of L, i.e., the instability sets in at all scales simultaneously; see Fig. 2.

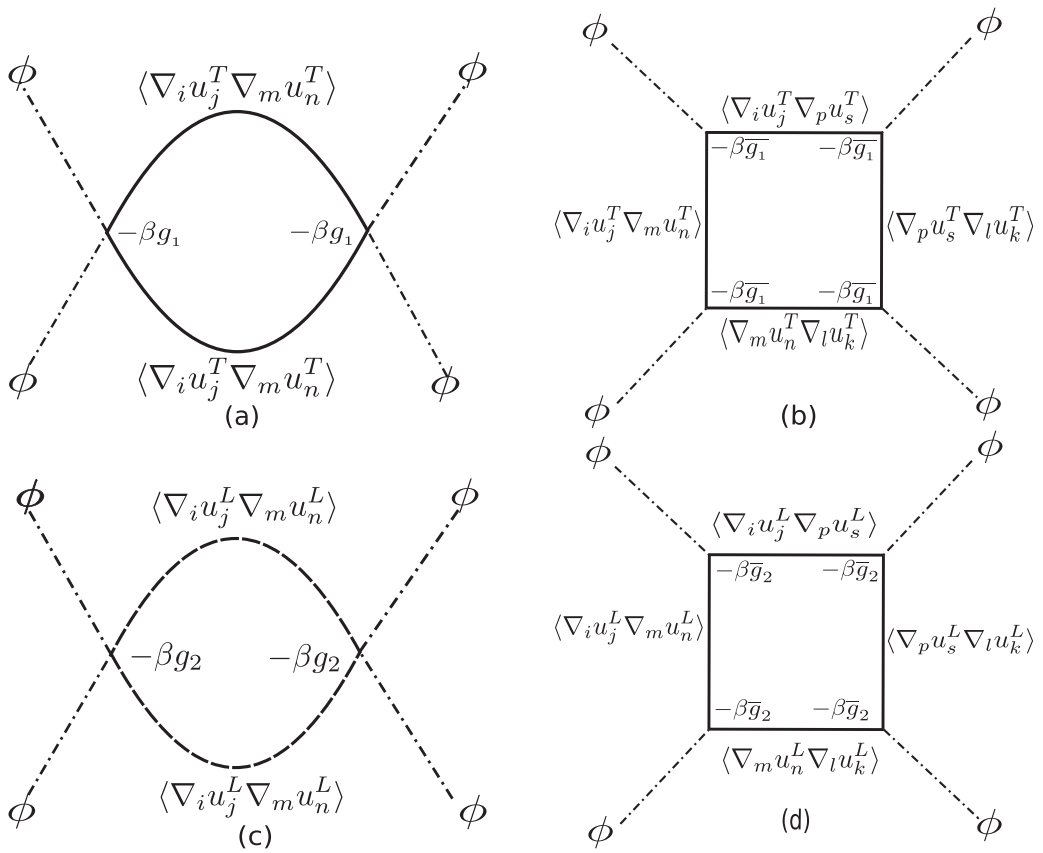

FIG. 18. One-loop inhomogeneous Feynman graphs that correct v.

In fact, for all positive (negative) $g_1 - \frac{\bar{g}_1^2}{2\mu}$, the positional correlation length L_c diverges (vanishes).

APPENDIX F: FIRST-ORDER TRANSITIONS

Consider the following diagrams that contribute to the one-loop corrections to v.

These diagrams are *finite*. For instance, Fig. 18(a) is given by

$$\beta_c^2 g_1^2 \int \frac{d^d q}{(2\pi)^d} \frac{T_c^2 q^4 \delta_{jm}\delta_{jm}}{4\mu^2 q^4} = 2d g_1^2 \frac{1}{4\mu^2} \int \frac{d^d q}{(2\pi)^d} = d g_1^2 \frac{1}{2\mu^2} \frac{\Lambda^d}{(2\pi)^d}. \tag{F1}$$

Similarly, Fig. 18(b) is given by

$$2\overline{\beta}_c^4 g_1^4 \int \frac{d^d q}{(2\pi)^d} \frac{T_c^4 q^8 \delta_{js}\delta_{sk}\delta_{kn}\delta_{nj}}{16\mu^4 q^8} = d\overline{g}_1^4 \frac{1}{8\mu^4} \frac{\Lambda^d}{(2\pi)^d}. \tag{F2}$$

Figure 18(c) is given by

$$\beta_c^2 g_2^2 \int \frac{d^d q}{(2\pi)^d} \frac{T_c^2 q^4 \delta_{jm}\delta_{jm}}{\tilde{\lambda}^2 q^4} = 2d g_2^2 \frac{1}{\tilde{\lambda}^2} \int \frac{d^d q}{(2\pi)^d} = 2d g_2^2 \frac{1}{\tilde{\lambda}^2} \frac{\Lambda^d}{(2\pi)^d}. \tag{F3}$$

Similarly, Fig. 18(d) is given by

$$2\beta_c^4 \overline{g}_2^4 \int \frac{d^d q}{(2\pi)^d} \frac{T_c^4 q^8 \delta_{js}\delta_{sk}\delta_{kn}\delta_{nj}}{\tilde{\lambda}^4 q^8} = 2d\overline{g}_2^4 \frac{1}{\tilde{\lambda}^4} \frac{\Lambda^d}{(2\pi)^d}. \tag{F4}$$

Neglecting the homogeneous fluctuation corrections, we obtain Eq. (96) above for v_e.

Consider the one-loop Feynman graphs in Fig. 19 that corrects g. These are all finite. Figure 19(a) is

$$\beta_c^3 4\overline{g}_1^3 \int \frac{d^d q}{(2\pi)^d} \frac{T_c^3 q^6 \delta_{js}\delta_{sn}\delta_{nj}}{16\mu^4 q^6}. \tag{F5}$$

Figure 19(b) is

$$\beta_c^2 2 g_1 \bar{g}_1 \int \frac{d^d q}{(2\pi)^d} \frac{T_c^2 q^4 \delta_{jm}\delta_{jm}}{4\mu^2 q^4}. \tag{F6}$$

Figure 19(a) is

$$\beta_c^4 4\overline{g}_2^3 \int \frac{d^d q}{(2\pi)^d} \frac{T_c^3 q^6 \delta_{js}\delta_{sn}\delta_{nj}}{\tilde{\lambda}^4 q^6}. \tag{F7}$$

Figure 19(c) is

$$\beta_c^2 2 g_2 \bar{g}_2 \int \frac{d^d q}{(2\pi)^d} \frac{T_c^2 q^4 \delta_{jm}\delta_{jm}}{\tilde{\lambda}^2 q^4}. \tag{F8}$$

Neglecting the homogeneous fluctuation corrections, we obtain Eq. (97) above for g_e. Here, $\beta_c = 1/T_c$.

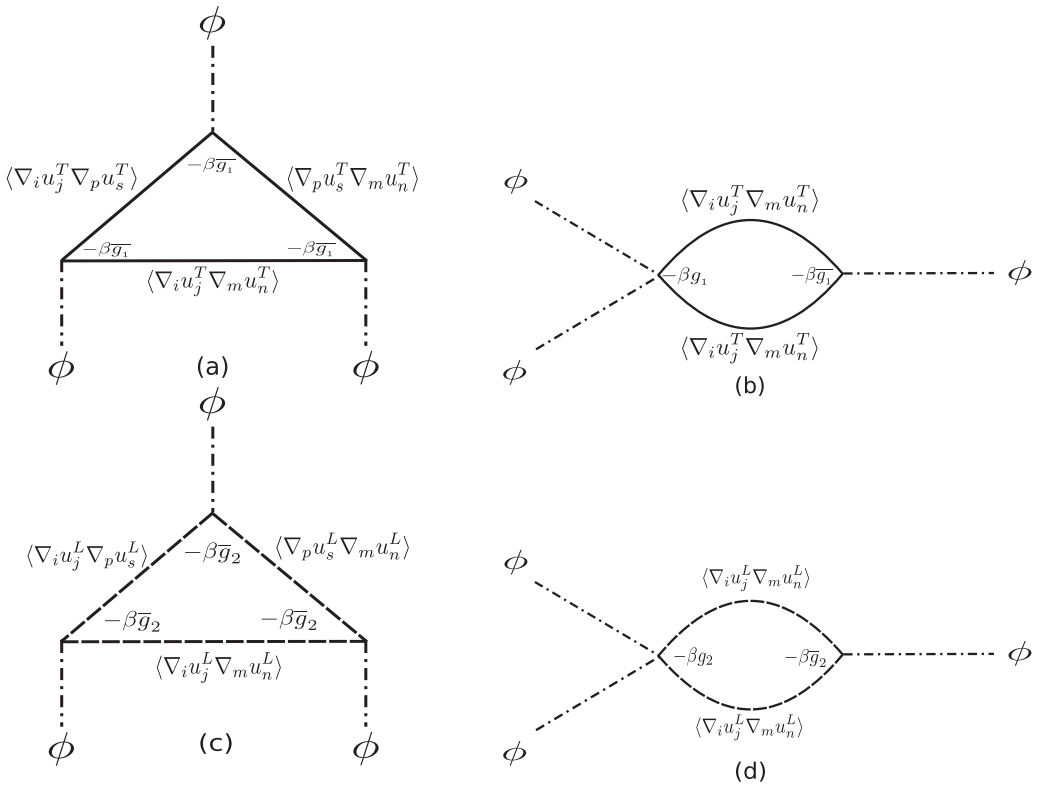

FIG. 19. One-loop inhomogeneous Feynman graphs that correct g.

[1] H. E. Stanley, *Introduction to Phase Transitions and Critical Phenomena* (Oxford University Press, Oxford, UK, 1987).

[2] S. K. Ma, *Modern Theory of Critical Phenomena* (Westview Press, Boulder, CO, 2000).

[3] S. K. Ma, *Statistical Mechanics* (World Scientific, Singapore, 1985).

[4] M. Plischke and B. Bergersen, *Equilibrium Statistical Physics* (World Scientific, Singapore, 2006).

[5] S. Safran, *Statistical Thermodynamics of Surfaces, Interfaces, and Membranes* (CRC Press, Boca Raton, FL, 2003).

[6] P. M. Chaikin and T. C. Lubensky, *Principles of Condensed Matter Physics* (Cambridge University Press, Cambridge, UK, 2000).

[7] C. P. Brangwynne, Soft active aggregates: Mechanics, dynamics and self-assembly of liquidlike intracellular protein bodies, Soft Matter **7**, 3052 (2011); A. A. Hyman, C. A. Weber, and F. Jülicher, Liquid-liquid phase separation in biology, Annu. Rev. Cell Dev. Biol. **30**, 39 (2014); A. Molliex, J. Temirov, J. Lee, M. Coughlin, A. P. Kanagaraj, H. J. Kim, T. Mittag, and J. P. Taylor, Phase separation by low complexity domains promotes stress granule assembly and drives pathological fibrillization, Cell **163**, 123 (2015); C. P. Brangwynne, P. Tompa, and R. V. Pappu, Polymer physics of intracellular phase transitions, Nat. Phys. **11**, 899 (2015).

[8] L. D. Landau, L. P. Pitaevskii, A. M. Kosevich, and E. M. Lifshitz, *Theory of Elasticity* (Butterworth-Heinemann, Oxford, UK, 1986).

[9] N. D. Mermin and H. Wagner, Absence of Ferromagnetism or Antiferromagnetism in One- or Two-Dimensional Isotropic Heisenberg Models, Phys. Rev. Lett. **17**, 1133 (1966); P. C. Hohenberg, Existence of long-range order in one and two dimensions, Phys. Rev. **158**, 383 (1967).

[10] Melting of a crystal in 3D is usually described by the well-known density functional theory [see, e.g., Y. Singh, Density-functional theory of freezing and properties of the ordered phase, Phys. Rep. **207**, 351 (1991)].

[11] B. I. Halperin and D. R. Nelson, Theory of Two-Dimensional Melting, Phys. Rev. Lett. **41**, 121 (1978).

[12] M. A. de Moura, T. C. Lubensky, Y. Imry, and A. Aharony, Coupling to anisotropic elastic media: Magnetic and liquid-crystal phase transitions, Phys. Rev. B **13**, 2176 (1976).

[13] D. J. Bergman and B. I. Halperin, Critical behavior of an Ising model on a cubic compressible lattice, Phys. Rev. B **13**, 2145 (1976).

[14] R. W. Style, T. Sai, N. Fanelli, M. Ijavi, K. Smith-Mannschott, Q. Xu, L.A. Wilen, and E. R. Dufresne, Liquid-Liquid Phase Separation in an Elastic Network, Phys. Rev. X **8**, 011028 (2018).

[15] K. A. Rosowski, T. Sai, E. Vidal-Henriquez, D. Zwicker, R. W. Style, and E. R. Dufresne, Nat. Phys. **16**, 422 (2020).

[16] X. Wei, J. Zhou, Y. Wang, and F. Meng, Modeling Elastically Mediated Liquid-Liquid Phase Separation, Phys. Rev. Lett. **125**, 268001 (2020).

[17] M. Kothari and T. Cohen, Effect of elasticity on phase separation in heterogeneous systems, J. Mech. Phys. Solids **145**, 104153 (2020).

[18] S. Biswas, B. Mukherjee, and B. Chakrabarti, Thermodynamics of droplets undergoing liquid-liquid phase separation, arXiv:2104.0065.

[19] See, e.g., L. Gu, B. Chakraborty, P. L. Garrido, M. Phani, and J. L. Lebowitz, Monte Carlo study of a compressible Ising antiferromagnet on a triangular lattice, Phys. Rev. B **53**, 11985 (1996); O. Tchernyshyov, R. Moessner, and S. L. Sondhi, Spin-Peierls phases in pyrochlore antiferromagnets, *ibid.* **66**, 064403 (2002); C. Weber, F. Becca, and F. Mila, Finite-temperature properties of frustrated classical spins coupled to the lattice, *ibid.* **72**, 024449 (2005); L. Pili and S. A. Grigera, Two-dimensional Ising model with Einstein site phonons, *ibid.* **99**, 144421 (2019).

[20] A. A. Hyman and K. Simons, Beyond oil and water-phase transitions in cells, Science **337**, 1047 (2012); C. F. Lee, C. P. Brangwynne, J. Gharakhani, A. A. Hyman, and F. Jülicher, Spatial Organization of the Cell Cytoplasm by Position-Dependent Phase Separation, Phys. Rev. Lett. **111**, 088101 (2013).

[21] D. Chen *et al.*, Phase transition and near-zero thermal expansion in $ZrFeMo_2$ VO_{12}, Phys. Lett. A **380**, 4070 (2016); R. Ohtani *et al.*, Zero in-plane thermal expansion in guest-tunable 2D coordination polymers, Inorg. Chem. **56**, 6225 (2017).

[22] S. Mukherjee and A. Basu, Stiffening or softening of elastic media: Anomalous elasticity near phase transitions, Phys. Rev. E **106**, L052102 (2022).

[23] G. Grinstein and R. A. Pelcovits, Anharmonic Effects in Bulk Smectic Liquid Crystals and Other "One-Dimensional Solids," Phys. Rev. Lett. **47**, 856 (1981); Smectic-A–C transition in three dimensions, Phys. Rev. A **26**, 2196 (1982).

[24] S. Leibler, Curvature instability in membranes, J. Phys. France **47**, 507 (1986); S. Leibler and D. Andelman, 1987. Ordered and curved meso-structures in membranes and amphiphilic films, *ibid.* **48**, 2013 (1987); T. Taniguchi, Shape Deformation and Phase Separation Dynamics of Two-Component Vesicles, Phys. Rev. Lett. **76**, 4444 (1996); T. Baumgart, B. R. Capraro, C. Zhu, and S. L. Das, Thermodynamics and mechanics of membrane curvature generation and sensing by proteins and lipids, Annu. Rev. Phys. Chem. **62**, 483 (2011); T. Banerjee and A. Basu, Thermal fluctuations and stiffening of symmetric heterogeneous fluid membranes, Phys. Rev. E **91**, 012119 (2015); N. Sarkar and A. Basu, Phase transitions and membrane stiffness in a class of asymmetric heterogeneous fluid membranes, J. Stat. Mech. (2015) P08023.

[25] Although single crystals are not isotropic, polycrystalline materials are macroscopically isotropic, which is due to the random orientations of the constituent crystallites. Similarly, gels are also isotropic at large enough scales.

[26] It is clear that if we replace $(u_{ij})^2$ by its average (which is nonzero), a linear term in ϕ is generated, with a coefficient that is the external magnetic field. Accessing the critical point would then require adding a suitable counter term in $\mathcal{F}$; see also later.

[27] The alert reader might wonder why a ϕ^3 is excluded. We did not include in a pure ϕ^3-term in $\mathcal{F}$, as we assumed a generic second order phase transition in the rigid limit ($\mathbf{u} = \mathbf{0}$), and assumed the existence of a second order transition even in the non-rigid case, which precludes a ϕ^3-term. Nevertheless, even if the microscopic free energy did not have a ϕ^3-term, it will be generated due to fluctuation effects. How a second order transition can still be accessed is discussed later in Sec. VI.

[28] Such selectivity is expected to be relevant in cell biological contexts, e.g., in interactions between the F-actin matrix in the cell cortex and the lipids attached to it. Such a system is however *active* or nonequilibrium, and hence our theory does not apply there directly.

[29] One can in-principle consider a superparamagnetic or ferromagnetic colloidal crystal, where the local displacements can couple with the two states of the magnetic spins *asymmetric* or *selectively*.

[30] A. T. Dorsey, P. M. Goldbart, and J. Toner, Squeezing Superfluid from a Stone: Coupling Superfluidity and Elasticity in a Supersolid, Phys. Rev. Lett. **96**, 055301 (2006).

[31] Equation (12) may be written schematically as $\hat{r} \equiv T - T_c^* = r + 2(\delta V/V)^2 \times \mathcal{O}(1)$. Very close to the critical point $\hat{r} \approx 0$, giving $dT_c/dV \sim \delta V$ that approaches zero in the limit of small δV.

[32] L. Onsager, Discussions, Nuovo Cim. **6**, 279 (1949).

[33] A. Pelissetto and E. Vicari, Critical phenomena and renormalization-group theory, Phys. Rep. **368**, 549 (2002); H. Kleinert, Critical exponents from seven-loop strong-coupling ϕ^4 theory in three dimensions, Phys. Rev. D **60**, 085001 (1999).

[34] H. Jeon *et al.*, Reducing the coefficient of thermal expansion of polyimide films in microelectronics processing using ZnS particles at low concentrations, ACS Appl. Nano Mater. **1**, 1076 (2018); A. Chandra *et al.*, Modifying thermal expansion of polymer composites by blending with a negative thermal expansion material, Macromol. Mater. Eng. **292**, 295 (2007); X. Song *et al.*, Adjustable zero thermal expansion in antiperovskite manganese nitride, Adv. Mater. **23**, 4690 (2011); F.-R. Shen *et al.*, Ultra-low thermal expansion realized in giant negative thermal expansion materials through self-compensation, APL Mater. **5**, 106102 (2017); S. Ando, M. Harada, T. Okada and R. Ishige, Effective reduction of volumetric thermal expansion of aromatic polyimide films by incorporating interchain crosslinking, Polymers **10**, 761 (2018); K. Takenaka, Progress of research in negative thermal expansion materials: Paradigm shift in the control of thermal expansion, Front. Chem. **6**, 267 (2018); J. Liu, H. E. Maynard-Casely, H. E. A. Brand, and N. Sharma, $Sc_{1.5}Al_{0.5}W_3O_{12}$ exhibits zero thermal expansion between 4 and 1400 K, Chem. Mater. **33**, 3823 (2021).

[35] J. Qu, M. Kadic, A. Naber and M. Wegener, Metamaterials with negative thermal-expansion coefficient from positive constituents, Sci. Rep. **7**, 40643 (2017); K. Wei, Additively manufactured bimaterial metamaterial to program a wide range of thermal expansion, Mater. Des. **198**, 109343 (2021).

[36] M. Takeuchi, H. Miyamoto, Y. Sako, H. Komizu, and A. Kusumi, Structure of the erythrocyte membrane skeleton as observed by atomic force microscopy, Biophys. J. **74**, 2171 (1998).

[37] D. H. Boal, Computer simulation of a model network for the erythrocyte cytoskeleton, Biophys. J. **67**, 521 (1994).